NAVAL POSTGRADUATE SCHOOL

MONTEREY, CALIFORNIA

THESIS

LASER PEENING FOR MITIGATION OF STRESS CORROSION CRACKING AT WELDS IN MARINE ALUMINUM

by

Heather R. Mattern

June 2011

Thesis Advisor:	Luke N. Brewer
Second Reader:	Joseph C. Farmer

Approved for public release; distribution is unlimited

THIS PAGE INTENTIONALLY LEFT BLANK

REPORT DOCUMENTATION PAGE			Form Approved OMB No. 0704-0188
Public reporting burden for this collection of information is estimated to average 1 hour per response, including the time for reviewing instruction, searching existing data sources, gathering and maintaining the data needed, and completing and reviewing the collection of information. Send comments regarding this burden estimate or any other aspect of this collection of information, including suggestions for reducing this burden, to Washington headquarters Services, Directorate for Information Operations and Reports, 1215 Jefferson Davis Highway, Suite 1204, Arlington, VA 22202-4302, and to the Office of Management and Budget, Paperwork Reduction Project (0704-0188) Washington DC 20503.			
1. AGENCY USE ONLY *(Leave blank)*	**2. REPORT DATE** June 2011	**3. REPORT TYPE AND DATES COVERED** Master's Thesis	
4. TITLE AND SUBTITLE Laser Peening for Mitigation of Stress Corrosion Cracking at Welds in Marine Aluminum		**5. FUNDING NUMBERS**	
6. AUTHOR(S) Heather R. Mattern			
7. PERFORMING ORGANIZATION NAME(S) AND ADDRESS(ES) Naval Postgraduate School Monterey, CA 93943-5000		**8. PERFORMING ORGANIZATION REPORT NUMBER**	
9. SPONSORING /MONITORING AGENCY NAME(S) AND ADDRESS(ES) N/A		**10. SPONSORING/MONITORING AGENCY REPORT NUMBER**	
11. SUPPLEMENTARY NOTES The views expressed in this thesis are those of the author and do not reflect the official policy or position of the Department of Defense or the U.S. Government. IRB Protocol number: N/A			
12a. DISTRIBUTION / AVAILABILITY STATEMENT Approved for public release; distribution is unlimited		**12b. DISTRIBUTION CODE** A	

13. ABSTRACT (maximum 200 words)

This work examines the use of laser peening (LP) for mitigation of stress corrosion cracking (SCC) in marine grade aluminum alloys (Al-Mg). These alloys can be sensitized during welding and will develop a tensile residual stress in the heat affected zone that may promote SCC in a salt water environment. Metal inert gas welded aluminum alloy 5083 (4.8wt% Mg) plate was laser peened using a variety of laser intensities to create compressive stresses. Mechanical tests were performed to investigate the SCC of the material including slow strain rate testing and potentiostatically driven, salt-water exposure. Microstructural and micromechanical tests were performed to characterize the effects of LP on the microstructure of the material. The slow strain rate testing showed a systematic decrease in ductility with increasing LP intensity. The fracture surfaces on all welded samples were indicative of ductile fracture but with a pre-crack length that scaled inversely with LP intensity. The hardness of the material increased with LP intensity. This work suggests that welded aluminum alloy 5083 does not readily stress corrosion crack. LP does affect the mechanical behavior of the material, but its full effect on stress corrosion behavior requires further study.

14. SUBJECT TERMS Stress Corrosion Cracking, Laser Peening, 5083 Aluminum Alloy			**15. NUMBER OF PAGES** 77
			16. PRICE CODE
17. SECURITY CLASSIFICATION OF REPORT Unclassified	**18. SECURITY CLASSIFICATION OF THIS PAGE** Unclassified	**19. SECURITY CLASSIFICATION OF ABSTRACT** Unclassified	**20. LIMITATION OF ABSTRACT** UU

NSN 7540-01-280-5500 Standard Form 298 (Rev. 2-89)
Prescribed by ANSI Std. 239-18

THIS PAGE INTENTIONALLY LEFT BLANK

Approved for public release; distribution is unlimited

LASER PEENING FOR MITIGATION OF STRESS CORROSION CRACKING AT WELDS IN MARINE ALUMINUM

Heather R. Mattern
Lieutenant Commander, United States Coast Guard
B.S., United States Coast Guard Academy, 1998

Submitted in partial fulfillment of the
requirements for the degree of

MASTER OF SCIENCE IN MECHANICAL ENGINEERING

from the

NAVAL POSTGRADUATE SCHOOL
June 2011

Author: Heather R. Mattern

Approved by: Luke N. Brewer
Thesis Advisor

Joseph C. Farmer
Second Reader

Knox Millsaps
Chair, Department of Mechanical and Aerospace Engineering

THIS PAGE INTENTIONALLY LEFT BLANK

ABSTRACT

This work examines the use of laser peening (LP) for mitigation of stress corrosion cracking (SCC) in marine grade aluminum alloys (Al-Mg). These alloys can be sensitized during welding and will develop a tensile residual stress in the heat affected zone that may promote SCC in a salt water environment. Metal inert gas welded aluminum alloy 5083 (4.8wt% Mg) plate was laser peened using a variety of laser intensities to create compressive stresses. Mechanical tests were performed to investigate the SCC of the material including slow strain rate testing and potentiostatically driven, salt-water exposure. Microstructural and micromechanical tests were performed to characterize the effects of LP on the microstructure of the material. The slow strain rate testing showed a systematic decrease in ductility with increasing LP intensity. The fracture surfaces on all welded samples were indicative of ductile fracture but with a pre-crack length that scaled inversely with LP intensity. The hardness of the material increased with LP intensity. This work suggests that welded aluminum alloy 5083 does not readily stress corrosion crack. LP does affect the mechanical behavior of the material, but its full effect on stress corrosion behavior requires further study.

THIS PAGE INTENTIONALLY LEFT BLANK

TABLE OF CONTENTS

LIST OF FIGURES

LIST OF TABLES

THIS PAGE INTENTIONALLY LEFT BLANK

LIST OF ACRONYMS AND ABBREVIATIONS

SCC – Stress Corrosion Cracking

LP – Laser Peening

AA5083 – Aluminum Alloy 5083 H116

MIG – Metal Inert Gas Welding

MIC – Metal Improvement Company

SSRT – Slow Strain Rate Testing

Ag-Mg - Aluminum alloys with magnesium

IGC - Intergranular Corrosion

IGSCC - Intergranular Stress Corrosion Cracking

HAZ – Heat-Affected Zone

THIS PAGE INTENTIONALLY LEFT BLANK

ACKNOWLEDGMENTS

First and foremost, I would like to thank Professor Brewer and his never-ending patience and enthusiasm. Both NPS and I are very lucky that he arrived when he did, and both better off because of his presence. I feel truly blessed that I get to say I was his first thesis student. I am positive there will be a long line of students to follow, and each one of them he will educate and inspire.

Dr. Farmer was a continual source of corrosion knowledge, which he shared freely and for that I am very grateful.

The following work would not have been possible without the technical expertise and generous collaboration of Dr. L. Hackel and C. Truong from Metal Improvement Company in Livermore, CA.

I would also like to thank Dr. J. Wolk and K. Tran from Carderock Division, Naval Surface Warfare Center for providing insight, knowledge and all of the welded material used in this research.

I would like to thank the professors and staff of NPS, who were so generous in sharing both their time and knowledge in both my thesis work and classroom studies: Dr. E. S. K. Menon, G. W. Young, Dr. A. Gannon, Dr. Papoulias, J. Mobley, Dr. C. Park, Dr. T. R. McNelley, LtCol R. Pollak and Dr. S. Sathe.

There were two parts in completing my degree, and I want to thank Aaron and Brian for making sure I got through the other one.

Finally, I would like to dedicate this to my colleagues and friends in Columbia.

THIS PAGE INTENTIONALLY LEFT BLANK

I. INTRODUCTION AND BACKGROUND

A. MOTIVATION

With rising fuel costs and the need to carry greater payloads, the marine industry; both commercial and military, is looking for ways to reduce the weight of ships without losing structural integrity. One of the leading ways the industry is combating this problem is with the use of strong lightweight materials. On average, aluminum is a third of the weight of steel. By building the topside structures from aluminum there can be considerable weight reduction of the overall ship. The fuel consumption of a ship can be approximated by:

$$\text{Fuel (F)} = [\text{Specific Fuel Consumption (SFC)}]*[\text{Specific Horse Power (SHP)}]*[\text{time(t)}] \quad (1)$$

$$F = kv^2\Delta^{2/3}$$

$k = \text{constant}$

$v = \text{velocity}$

$\Delta = \text{displacement}$

Therefore:

$$\frac{F_{Al}}{F_{Steel}} = \left(\frac{\Delta_{Al}}{\Delta_{Steel}}\right)^{2/3}$$

$$\left(\frac{V_{Al}}{V_{Steel}}\right)^2 = \left(\frac{\Delta_{Steel}}{\Delta_{Al}}\right)^{2/3}$$

$$\frac{Range_{Al}}{Range_{Steel}} = \left(\frac{\Delta_{Steel}}{\Delta_{Al}}\right)^{2/3} \quad (2\text{-}4)$$

For example, as shown in Figure 1, if the weight of a ship were reduced by 15%, then the approximated reduction in fuel consumption would be 10%, the possible increase in speed with the same amount of fuel would be 5.6% or the possible increase in range with the same amount of fuel would be 11.4%.

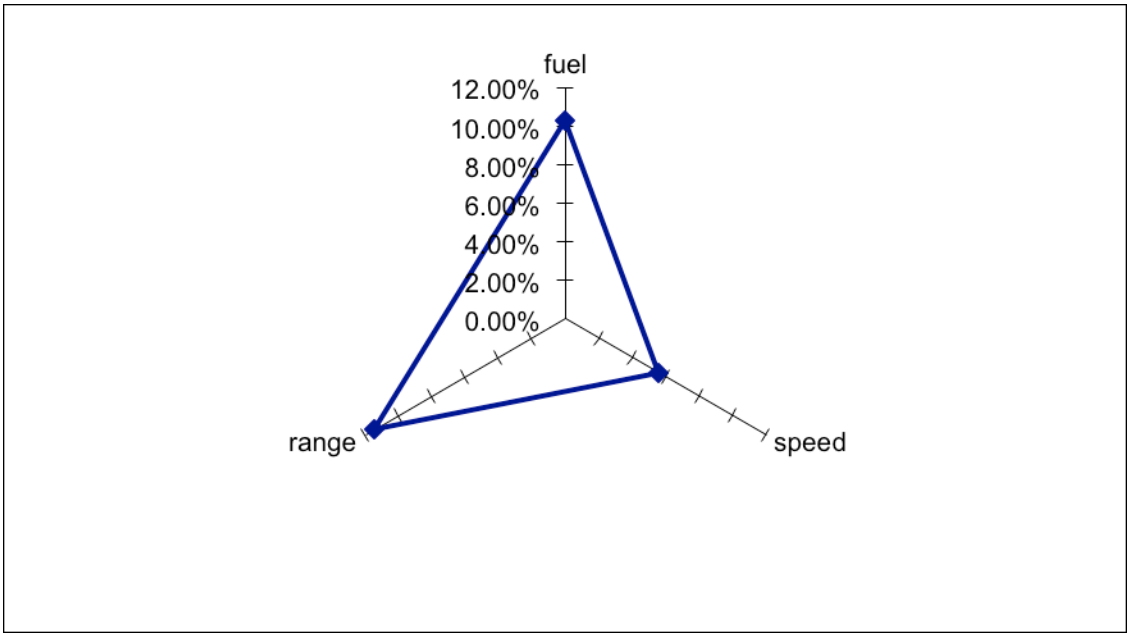

Figure 1. Comparison of amount fuel, range or speed increase with a 15% reduction in weight.

1. Aluminum in Marine Structures

Despite these potential benefits, aluminum structures in marine environments have demonstrated susceptibility to stress corrosion cracking (SCC). In 2001–2002, over 400 aluminum vessels that ranged from 4 to 44 meters, plus additional fuels tanks, were constructed using aluminum alloy 5083-H321 (4.7 weight percent magnesium). Shortly after being put in service, both industry and Coast Guard inspectors noticed severe pitting and extensive SCC, eventually leading to condemning the hulls of all the vessels. Upon this discovery, the Aluminum Solution Team (AST); overseen by the Coast Guard, completed an investigation of the problem. It was found that the vessels were all built out of single batch of aluminum that had been sensitized, a condition that occurs when the aluminum-magnesium alloys are exposed to elevated temperatures for extended period of time. The AST helped to write a new ASTM standard (B928) specifically for assessing sensitization in marine grade aluminum, which included required testing for plate aluminum. This new standard has reduced the number of incidents to SCC in

aluminum hull vessels. However, this new standard does not completely eradicate the problem, and the question of sensitization of 5xxx series aluminum alloys during operation or the construction process still remains [1].

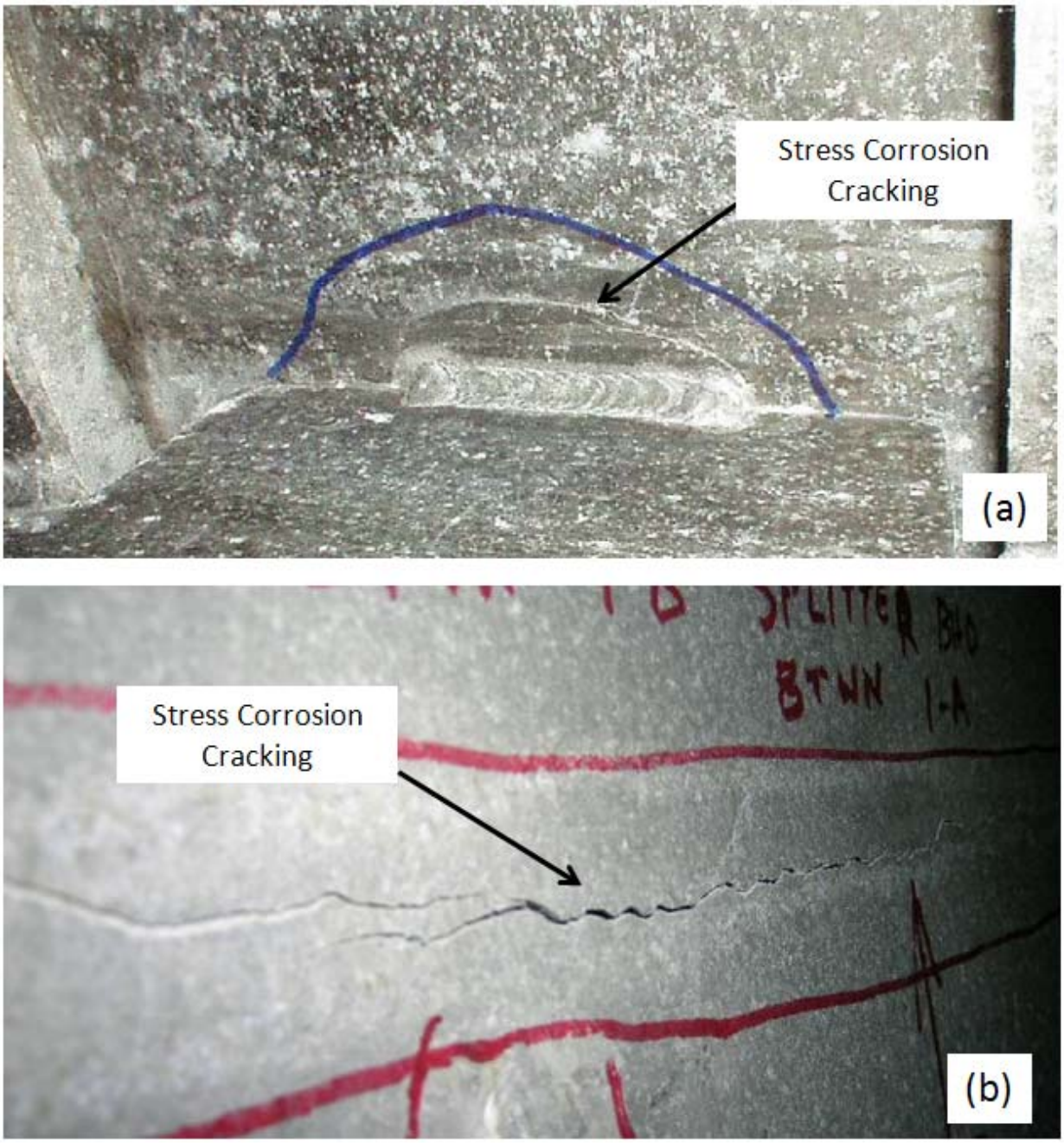

Figure 2. Stress corrosion crack around weld in (a) AA5083 plate found in a commercial vessel (From [1]) and (b) SCC in AA5456 (photograph courtesy W. Goins, NSWCCD).

Currently, the Navy has 22 Ticonderoga class cruisers (CG 47) that are operating with existing SCC that have [2] generated cracks in the superstructures, some up to nine feet in length (Figure 2). Replacement for all 22 superstructures would be both a costly endeavor for the Navy and each vessel would have to be removed from service for an extended dry dock period in order to complete the retrofit [2]. On board the USS PORT ROYAL, during operations in the Pacific Northwest, the crew discovered cracks in superstructure, some as high as the 06 level. The cracks were severe enough that the vessel was sent to Pearl Harbor for a $14 million extend repair period. There have been more than 3,000 cracks found on the Ticonderoga class fleet. The most prevalent places are the areas exposed to elevated temperatures caused by solar absorption and exhaust temperatures. The superstructures are made out of AA5456, a material that is quite prone to SCC because of it high magnesium content (5.1 wt %) [3].

In addition, the U.S. Navy has shown a renewed interest with marine grade aluminum construction and currently two classes of ships, the littoral combat ships (LCS) and the American class amphibious assault ships (LHA) are being built using AA5083 in the superstructures. AA5083 has a history of SCC and in order to prevent future expensive down time and repairs the Navy must have a better understanding on preventing and mitigating SCC damage in structural components, in order to not to repeat the condition of the Ticonderoga class [4].

2. Mechanism of Stress Corrosion Cracking

SCC requires that three conditions be met simultaneously: susceptible metallurgy; corrosive environment; and tensile stress (Figure 3). In regard to environments known to cause SCC, electrolytes with halide anions cause SCC in many Fe-, Al- and Ni-based alloys, as well as in other alloy systems. SCC can initiate at a surface flaw, such as a corrosion pit, that serves as a stress riser—the critical flaw size can be calculated from the threshold stress intensity factor for stress corrosion cracking. The propagation of SCC involves three stages: (1) initiation or incubation; (2) propagation; and (3) failure or arrest. The brittle fracture experienced during SCC is related to the formation of a brittle phase at the crack tip—propagation occurs during the periodic rupture of this brittle

phase. Since the brittle phase is an oxide that can be predicted with the corresponding Pourbaix diagrams, SCC can be correlated with specific combinations of pH and potential. Various crack propagation models exist, including (1) the film rupture model and (2) the slip-dissolution-repassivation model. SCC can be accelerated with increased tensile stress, increased temperature, increased applied potential, increased halide anion concentration, increased levels of dissolved oxygen, and either extremely acidic or alkaline pH. SCC can be mitigated by removing the corrosive environment, introducing inhibitor ions, using a material not susceptible to SCC in the service environment, and by the removal of residual tensile stress around welds or in areas experiencing fatigue (in cases of corrosion fatigue) through peening.

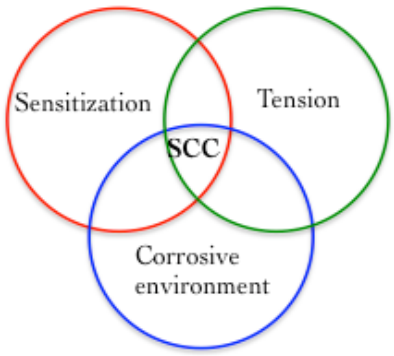

Figure 3. Venn diagram showing the mutual importance of sensitization, stress, and corrosive environment for stress corrosion cracking.

SCC is especially dangerous because it can occur at stresses within typical design ranges. The cracks can appear to be brittle fractures even though they are happening in a ductile material and are the result of local corrosion. Cracks can be either intergranular or transgranular; but for sensitized AA5083, they proceed primarily by intergranular cracking [5]. The tensile stress can result from various sources: applied, residual, thermal or welding. Normal ship motion, hogging and sagging, creates continues cyclical compressive and tensile stresses. Forces from water, wind, machinery and payload create a dynamic stress environment on the ship. In addition, welded metal can often have residual stresses near the yielding point and is a common source of SCC. The tensile

stresses are not along the weld bead but directly beside it along the heat-affected zone (HAZ.) As the welded material and the HAZ is heated and then cooled, its expansions and contraction are limited by the unaffected base material; therefore leaving the welded area and the HAZ in tension and the surround base metal in compression [6]. Figure 4 shows the residual stress of a MIG weld in AA5083-H321. Notice that the highest amount of residual tensile stress is in the HAZ [7]. The tensile stresses can crack the oxide passivation layer formed on the aluminum surface and make a crack intuition site.

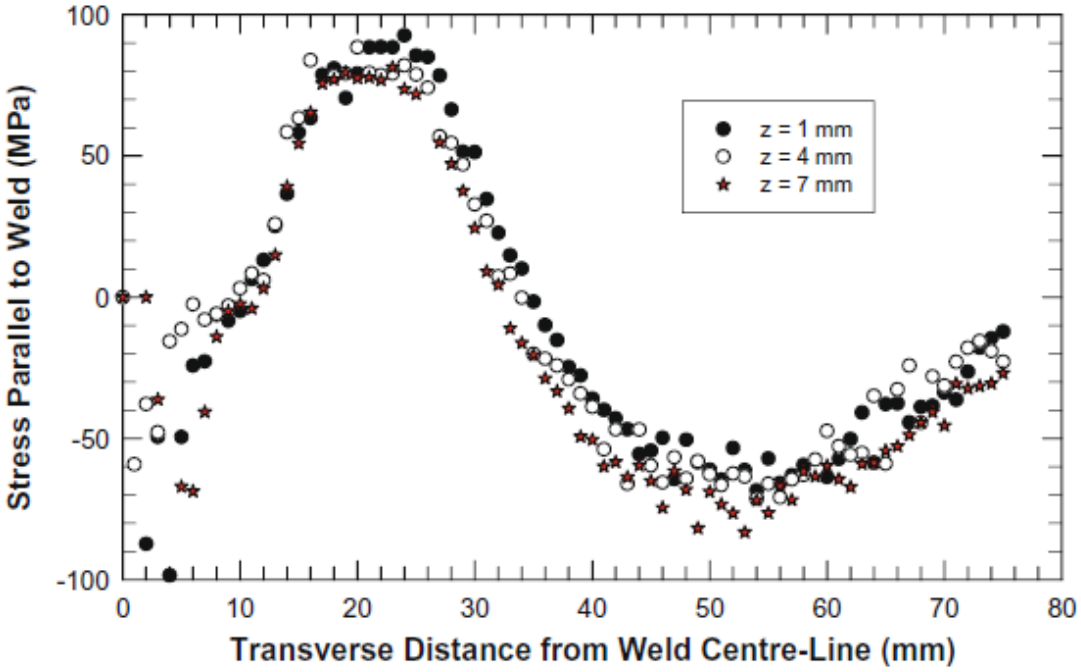

Figure 4. Comparison between longitudinal stresses in AA5083-H321 MIG weld (From [7]).

James et al. confirmed the extent of residual stress after metal inert gas (MIG) welding of AA5083-H321 [7]. The peak transverse stresses varied from +50 MPa at the heat affected zone, which is 19% of the parent plate strength, to -150 MPa at the weld centerline, which is 57% of the parent plate strength. The longitudinal stresses were +90 MPa, 22 mm from the weld centerline, 34% of the parent plate strength, to -120 MPa at the weld centerline, 45% of parent plate strength (Figure 5).

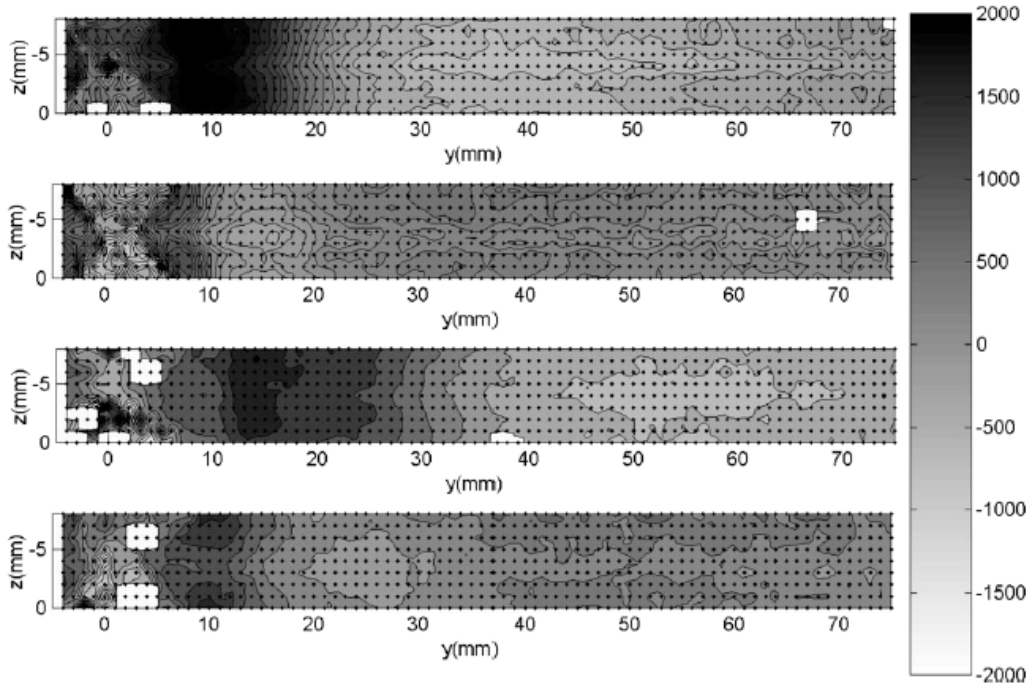

Figure 5. Variation of residual strain in the x and y directions for both the low heat input (LI) and high heat input (HI). From top to bottom: LI x-direction, LI y-direction, HI x-direction and HI y-direction (From [7]).

Not surprisingly, saline water is a corrosive environment for aluminum and its alloys. Alloys exposed continuously to salt water solution often have less evidence of corrosion then that of the same alloy exposed to alternating wet and dry environment. This is a crucial point for ships because of not only the wind-water line on the hull but because of the areas that see an increase in moisture during rough seas or humid conditions and then dry off while in port or in the sun. Aluminum alloys with a large amount of magnesium are more susceptible to SCC perpendicular to the rolling direction, because of the way precipitates are distributed during the rolling process. Aluminum is often used because under normal conditions, fresh water with a pH of 4.0 to 8.5, it naturally forms a protective, passivating oxide film. The film is self-renewing so if there is an abrasion or other damage on the surface the film is rapidly repaired. In order for the aluminum alloy to corrode there must be continuous film abrasion or the conditions of the surface must degrade the oxide film. Salt water, which typically has 3.5% NaCl,

provides the proper conditions for the corrosion of aluminum alloys. The Cl^- combined with the positive Al^{3+} ions leave holes in the oxide film where corrosion can initiate [5].

3. Incorporation of SCC Effects Into Fracture Mechanics

The above discussion concerning SCC must be reflected in the fracture mechanics model used to predict the propagation of SCC flaws and the final failure of a component. In addition to tensile stress, a susceptible microstructure, and a material-specific corrosive environment, a flaw must exist which is capable of nucleating into a stress corrosion crack and propagating to failure [8]. Flaws can either pre-exist due to poor manufacturing practices, or be initiated at locations where high stress concentration exists, such as grooves and corrosion pits. Once a crack is initiated, the crack will grow by SCC when the applied stress intensity factor, K_I, is equal to or larger than SCC resistance parameter, K_{ISCC}.

$$K_I \geq K_{ISCC} \tag{5}$$

The stress corrosion cracking resistance parameter, K_{ISCC} is a material and environment dependent property; which can be obtained through fracture mechanics testing of the materials in the specified environment. Final fracture will occur when the stress corrosion crack has achieved the critical crack length, thus making $K_I > K_{IC}$.

SCC models require knowledge of K_I as a function of crack length. The calculation of K_I requires knowledge of the stress field at the crack tip and the crack length at a given time.

$$K_I(a,\sigma) = \beta\,\sigma\sqrt{\pi\,a} \tag{6}$$

In this equation, β is a factor dependent on the shape (geometry) of the crack and the configuration of the structural component, and σ is the tensile stress. In most cases of practical importance, closed-form solutions are not available for evaluating K_I since the stress σ may be non-uniformly distributed, and since the geometry factor β is a function of crack size. Closed-form solutions are possible in some ideal cases involving uniform tensile stress and simple geometry, such as the classical problem of a single-edge cracked

plate with thickness *h*. Since stresses are non-uniformly distributed in most practical problems, the stress intensity factor has to be calculated through application of numerical algorithms (finite element model).

Using the fracture criterion for SCC and the expression for the stress intensity factor, the critical flaw size for SCC initiation and propagation can be derived:

$$a_{critical} \geq \frac{1}{\pi}\left(\frac{K_{ISCC}}{\sigma_{yield}\beta(a,h)}\right)^2 \tag{7}$$

In the end, the crack length, a, will grow as a function of time in an SCC environment. Prediction of final fracture requires an ability to predict the crack growth rate.

Several models have been developed to provide predictive capability for the crack length as a function of time, a(t). The formulation of such a model of crack propagation requires the choice of a working hypothesis for the cracking mechanism and the evaluation of the parameters of importance in the mechanism. Historically, environmental cracking has been separated into "initiation" and "propagation" phases. This distinction is almost always arbitrary, for initiation is invariably defined as the time at which a crack is detected, or when the load has relaxed a specific amount (in a strain-controlled test); in these cases, initiation generally corresponds to a crack depth of significant metallurgical dimensions (e.g., 2 mm). One of the more widely applied models is the slip dissolution or film rupture mechanism. This cracking mechanism has been successfully applied to model the SCC for stainless steel, low-alloy steel and nickel-based alloys in light water reactor environments. [8] The slip dissolution model shows the dependence of crack propagation rate (V_t) on the crack tip strain rate ($\dot{\varepsilon}_{ct}$) and is represented by the following equation:

$$V_t = A\left(\dot{\varepsilon}_{ct}\right)^n \tag{8}$$

where V_t has the unit of cm s^{-1} and $\dot{\varepsilon}_{ct}$ has the units of s^{-1}. The crack tip strain rate, $\dot{\varepsilon}_{ct}$, in equation 8 is related to the engineering stress (or stress intensity). The parameters *A* and *n* depend upon the material and environment at the crack tip. These two parameters

can be determined from the measured rate of repassivation. Such measurements are made by rapidly straining wires that are fabricated from the material of interest.

Considering:

$$velocity = \frac{distance}{time} \text{ and therefore: } time = \frac{distance}{velocity},$$

the time to failure, $t_{failure,}$ can be defined by substituting in Equation 8:

$$t_{final} = \frac{a_{critcal} - a_0}{V_t} = \frac{\pi\left(\frac{K_{IC}}{\beta\sigma}\right)^2 - a_0}{A(\dot{\varepsilon}_{ct})^n} \tag{9}$$

and by assuming the initial crack size, $a_{0,}$ is zero and solving for K_{IC}:

$$K_{IC} = \left(\frac{t_f A(\dot{\varepsilon}_{CT})^n}{\pi}\right)^{1/2} \beta\sigma \tag{10}$$

The K_{IC} value is proportional to the crack tip strain rate to the n/2 power.

4. Aluminum and Stress Corrosion Cracking

Aluminum alloys with magnesium (Ag-Mg), 5xxx series, are a good choice for vessel construction because of their moderate strength, formability, weldability and excellent general corrosion resistance. The 5xxx alloys are non-heatreatable and their primary strengthening mechanism is through the addition of magnesium in solid solution. The 5xxx series alloys exhibit good general corrosion resistance, especially when the magnesium is kept in solid solution [9]. However, alloys that contain more than 3 wt% magnesium can become susceptible to both intergranular corrosion (IGC) and intergranular stress corrosion cracking (IGSCC) when exposed to temperatures above 50ºC (122ºF) in a corrosive environment for a sufficient length of time [10]. Prolonged exposure to elevated temperature causes segregation of excess magnesium to the grain boundaries, resulting in the precipitation of the β phase (Al_2Mg_3), which is anodic to the grain interiors (Figure 6). The decrease of the magnesium in the solid solution base metal also causes a loss in tensile strength and hardness.

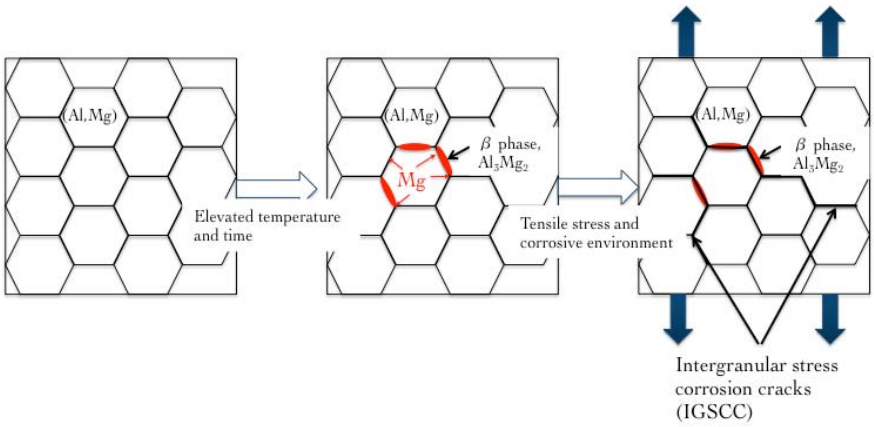

Figure 6. Schematic showing the process of sensitization in Al-Mg alloys and how it leads to SCC.

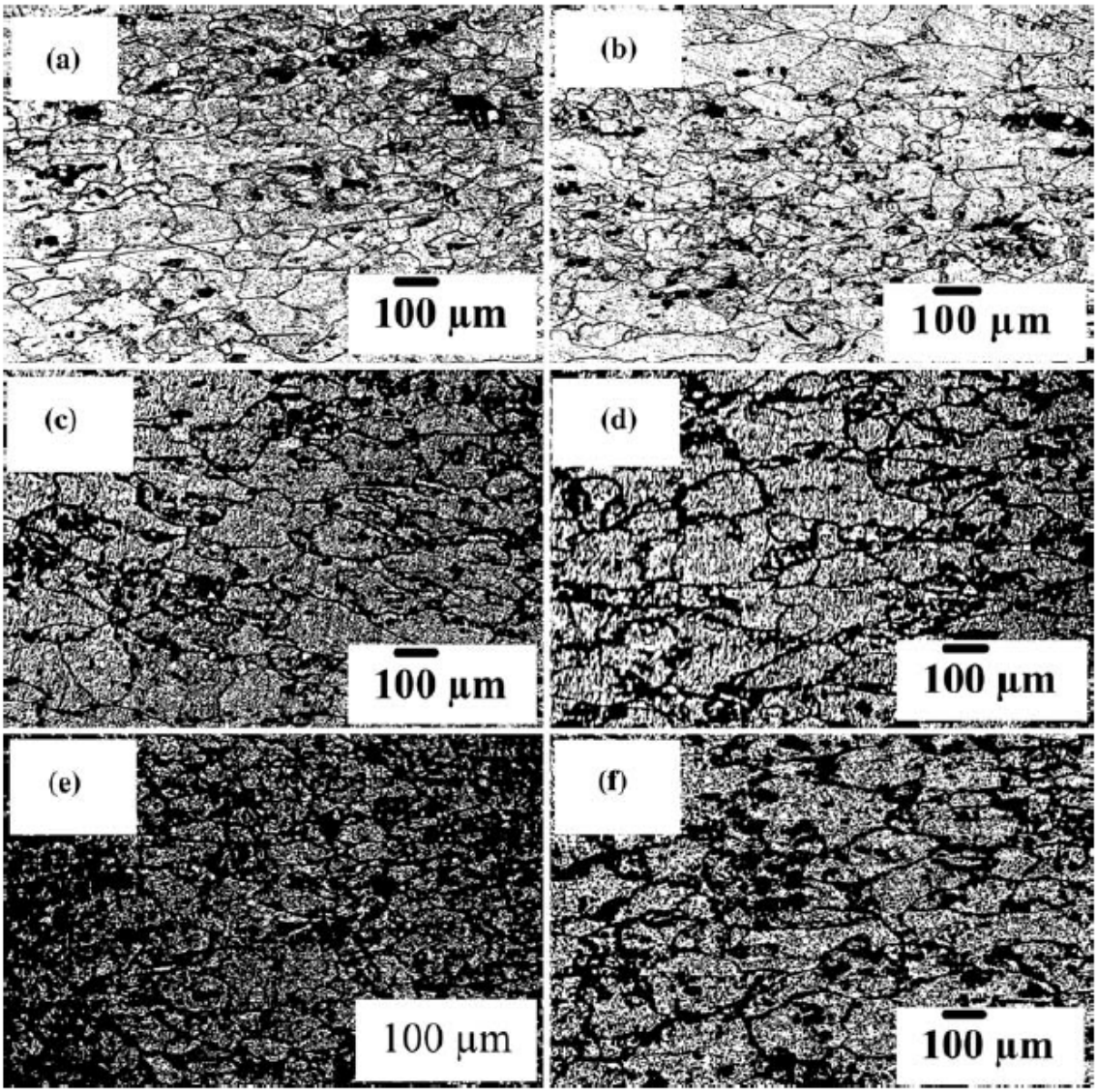

Figure 7. Optical micrographs showing the effect of sensitization heat treatment on the microstructure of as received specimen and specimens sensitized at 175ºC for different lengths of time: (a) as received (b) 24 h, (c) 168 h, 9d) 336 h, (e) 504 h, (f) 672 h (From [10]).

Oguocha et al. studied the effects of sensitization heat treatment on AA5083-H116 [10]. The properties of the sensitized material and the as-received material were investigated by using both mechanical testing and microscopy investigation. Sensitization resulted in a decrease in both chemical and mechanical properties of the alloy with increasing sensitization temperature and time, with the maximum effects

observed for an anneal of 175ºC for 672 hours. Susceptibility to intergranular corrosion (IGC) was measured using the nitric acid mass loss test (NAMLT) [11]. The NAMLT testing showed a clear increase in IGC with increasing exposure to temperature and time and was attributed to the formation of magnesium rich particles (β phase) at the grain boundaries. When the magnesium migrates to the grain boundaries it also decreases the amount in solid solution causing softening and a loss in tensile strength and hardness properties. Recrystallization at elevated temperatures also contributed to the loss in tensile and hardness properties (Figure 7).

Zucchi investigated the corrosion behavior of friction stir welded (FSW) joints compared to MIG welded joints. [9] Pitting and SCC resistance was determined in 3.5% NaCl + 0.3 f/l H_2O_2 and EXCO (4M KCl + O.5 M KNO_3 + 0.1 M HNO_3) solutions. Slow strain rate test (SSRT) at $1x10^{-6}$ s^{-1}, was used to measure SCC susceptibility. The MIG-welded joints were susceptible to SCC and cracked in both solutions while the FSW joint welds did not.

In order to reduce SCC, aluminum alloys such as AA5083 alloy with a H116 temper are specially rolled to avoid grain boundary precipitation, thus reducing its susceptibility to SCC. However, this specific heat treatment can still be vulnerable to sensitization when exposed to high temperatures for extended amounts of time in a corrosive environment.

As discussed by R. H. Jones and R. E. Ricker [8], critical potentials for the initiation of SCC can be related to potential-pH stability diagrams, since these diagrams can be used to predict the local environmental conditions required for formation of the brittle oxide phase at the crack tip, generally believed to be one of the necessary conditions for SCC. Jones [8] also shows the relationship between cyclic polarization curves and regions of potential where SCC is known to initiate and propagate in other alloys systems, such as austenitic Alloys 600, 800, and AISI type 304 stainless steel. Potential zones of susceptibility for both intergranular stress corrosion cracking (IGSCC) and transgranular stress corrosion cracking (TGSCC) of these austenitic alloys are shown.

Such electrochemical driving forces are also important for the initiation of IGSCC in aluminum based alloys such as AA5083. Jones [12] goes on to discuss the importance of the "solution potential" for various aluminum alloys in his chapter on aluminum-alloy SCC. This potential is said to be primarily determined by the composition of the aluminum-rich solid solution in such alloys. He gives the solution potential for AA5083 as -870 mV vs. the saturated calomel electrode (SCE). The importance of β-phase precipitates (Al_3Mg_2) at or near grain boundaries in the mechanism of intergranular corrosion and SCC of aluminum alloy 5083 is also discussed in detail by Jones (Figure 8), with the recognition that the preferential anodic dissolution of these precipitates at the corrosion potential can lead to severe problems. Note that other phases such as Al_8Mg_5 may also exist.

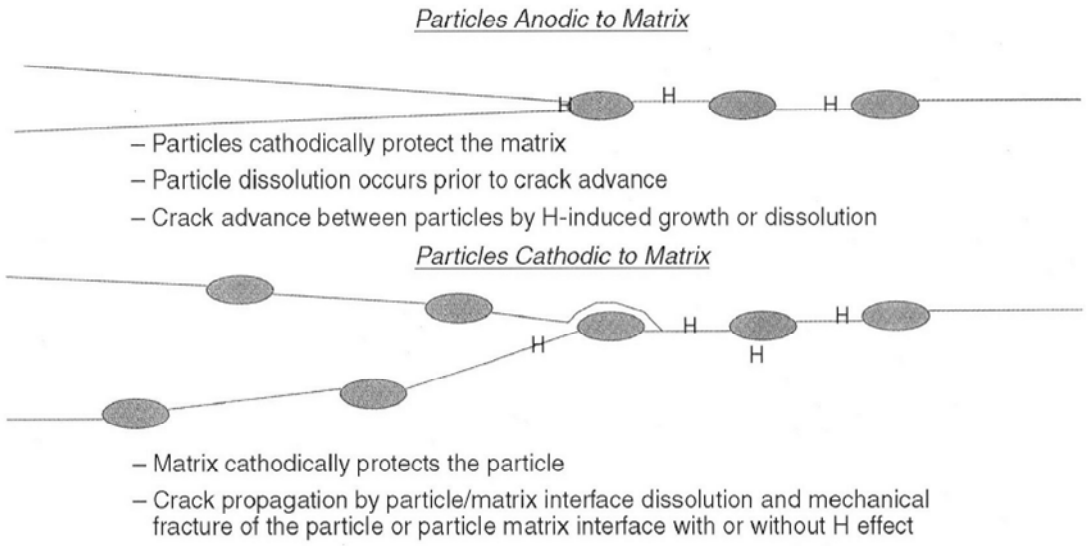

Figure 8. Schematic showing possible crack-tip/particle interactions for electrochemically active particles (From [9]).

B. METHODS FOR COMBATING SCC IN ALUMINUM

1. Non Stress Methods

One way to reduce the susceptibility of SCC is to make the material more corrosion resistant by altering its composition and/or heat treatment. Reducing the amount of amount of magnesium to less than 3 wt% would remove the problem of

sensitization, but the alloy would lose its strength, which is needed in ship structures. Aluminum has been chosen primarily for its light weight. A lower-strength alloy will require thicker sections to maintain the required load capacity, thus nullifying the attractiveness of aluminum.

Another option for combating SCC, widely used in the marine industry, is painting and coating. The coating approach is a viable option but should used in addition to other measures. On a working ship coatings can often become damaged leaving exposed material that will be more susceptible to corrosion than left unpainted. With a small exposed area of metal there would be a small anode and a larger cathode resulting in a larger corrosion rate in the pitted area. In addition, poor adhesion between the paint and the substrate can lead to the formation of blisters in the coating and the subsequent initiation of filiform corrosion and deep pitting.

2. Reduction of Stresses

It is not possible to prevent a ship from hogging and sagging and other flexural movement caused by the dynamic shipboard environment. The other option is to reduce the residual stresses due to welding. One way of reducing stress is careful fit-up during construction and repairs. Good welding practices such as rounding the corners of a patch will also reduce stress in the welds. A technology that is becoming more popular is friction stir welding (FSW). FSW is a solid state process that joins two pieces of metal but does not melt them in the process. By reducing the amount of heat added during the process and by avoiding fusion of the metals involved, FSW exhibits less tensile residual stress and a more refined microstructure when compared with the welded microstructure produced by traditional fusion welding methods. In addition, no filler material is used; so the original base material is continuous throughout the weld [9]. This technology is becoming more widely used in the marine industry; and though well suited for some aspects of initial construction, it would be problematic in repair procedures. It also cannot alleviate the SCC in existing material.

3. Compressive Stress Methods

One of the most effective methods of preventing SCC due to residual tensile stress is by imposing a residual compressive stress. Residual compressive stresses are often introduced by local plastic deformation. The compressive stress helps prevent new cracks from initiating and existing cracks from propagating by forcing the material together. The three most common methods are ultrasonic impact treatment (UIT), shot peening, and laser peening [13].

UIT uses continuous ultrasonic vibrations transferred through a hardened material tip that is placed in continuous contact with the treated surface. The near surface of the material experiences a high-rate, plastic straining and heating during the impact, resulting in a surface compressive stress (Figure 9). The compressive residual stresses tend to be more stable than those of shot peening [14].

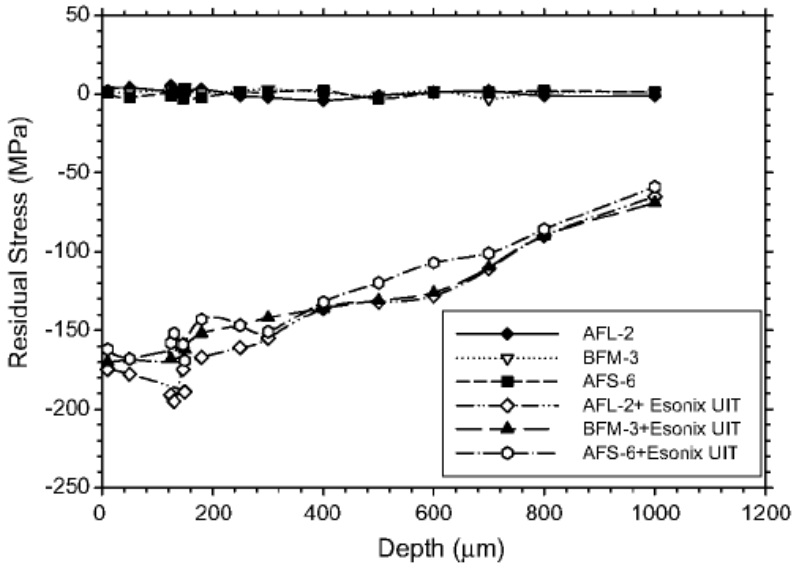

Figure 9. Residual stress distribution prior to and after the *Esonix* UIT on lightly (AFL-2), moderately (BFM-3), and severly (AFS-6) exfoliated 7075-T6511 specimens. (From [14]).

Shot peening is a process in which small, hard particles (glass or metal spheres), with diameters in the range of 0.1 to 1.0 mm are projected at high velocities onto the surface to be treated. The resulting impacts on the surface create residual compressive

stress to a depth of one-quarter to one-half of the shot diameters [13]. The pattern projected is random and therefore, it is impossible to ensure 100% coverage of the area being treated. The depth of the compressive layer averages around 250 μm, which is relatively shallow compared to most plate thicknesses in practical use.

Laser peening is a process that builds on the shot peening approach but uses a high intensity laser beam in lieu of hard particles. The laser beam, often a high-energy pulsed neodymium (Nd) glass laser, delivers a compressive stress on the surface of the work piece (Figure 10). The surface of the piece is turned into a plasma during the process and can double as a paint removal process. Next, a tamping layer, most often flowing water, is needed. After the laser strikes the surface, the beam is absorbed and forms high intensity plasma. The plasma is laterally confined by the tamping layer and a pressure buildup of several gigapascals is created at the surface [4]. The ensuing shock wave produces extensive plastic deformation of the material. The plastic deformation, in turn, results in a large, compressive residual stress in the material. Traditionally, the surface is covered with an absorption layer (paint or tape) but recently the trend is not to use the layer but to instead increase the intensity of the laser. This new approach reduces the amount of man-hours but maintains the same degree of intensity of the peening process.

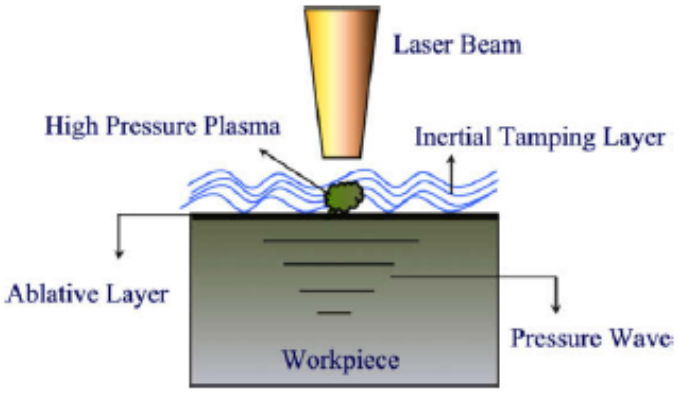

Figure 10. Laser Peening Process (From [15]).

The material of the work piece and the processing conditions used will determine the actual depths of the LP-induced stresses. The parameters that determine the depth of

the affected zone are the laser's power, spot size on target, duration of the shock, number shocks, and type of confining medium and absorptive layer. LP obtains eight to ten times deeper compressive residual stress than traditional shot peening. Other advantages of LP are that the surface of the work piece remains virtually unaltered and the temperature of the material only rises to 149ºC for a short time. LP has shown in various applications to enhance fatigue strength and SCC resistance. In addition, LP is being used to form shapes such as aircraft wing skins [4]. LP has primarily been used in the aircraft industry where it has increased the longevity of aircraft components by making them more resilient to cyclic loading and environmental conditions. The aircraft parts for which LP is in wide use include turbine blades, aircraft structural components such as landing gear and other components with notches, and holes and corners that are prone to fatigue failure. LP has been identified as a solution to critical SCC problems for canisters filled with nuclear reactor waste of the Department of Energy's Yucca Mountain Nuclear Waste Disposal Program. Laser peening as a method of mitigating SCC at the final closure welds was first demonstrated for the high-level waste program in the United States (Figure 11) [16].

The widespread application LP has been limited to date by high instrument costs and the relatively slow process rate. Recent laser technology developments have increased the processing speeds and repetition rate with better beam uniformity leading to increased industrial possibilities for the technology.

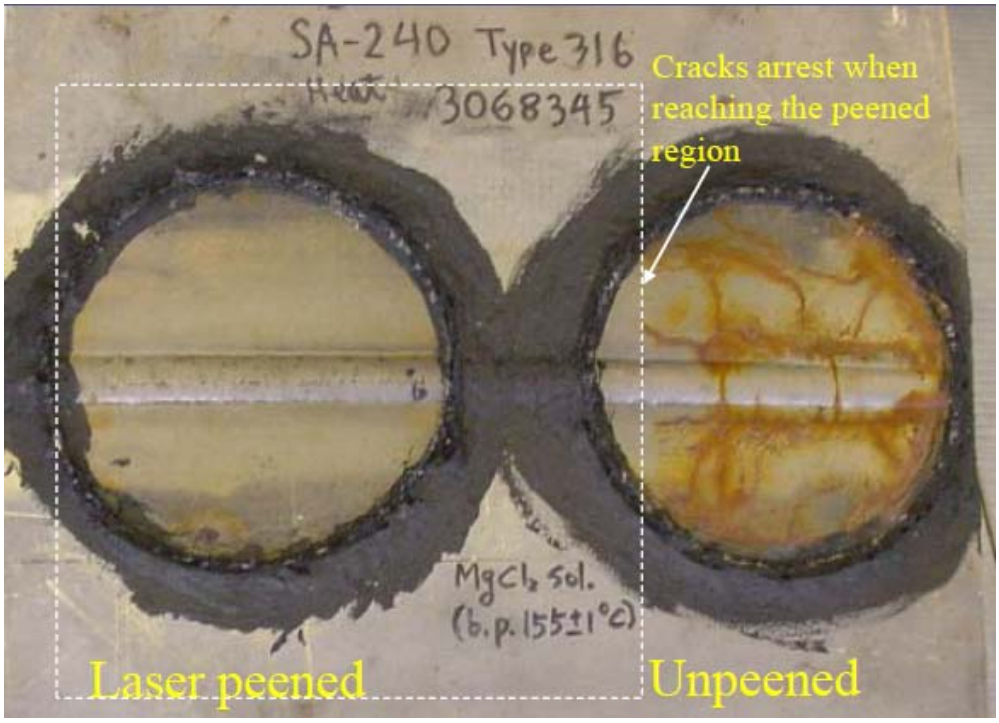

Figure 11. Corrosion testing of peened and unpeened 316 stainless steel done and tested at Lawrence Livermore National Laboratory as part of the high-level waste program [Francis T. Wang et al. LLNL]. Figure provided by Metal Improvement Company, a licensee of LLNL. Notice lack of SCC in peened sample. (From [16]).

Tran et al. investigated the improvement of fatigue life of lightweight alloys after LP [4]. It was found that the application of compressive residual stresses in the metal surface significantly improve fatigue life of as welded samples (Figure 12). The initial research shows that LP is an effective technology for enhancing the fatigue life of AA5059-H116, titanium Ti-5111, and high nickel alloy MP35N, all used as Navy light weight alloys.

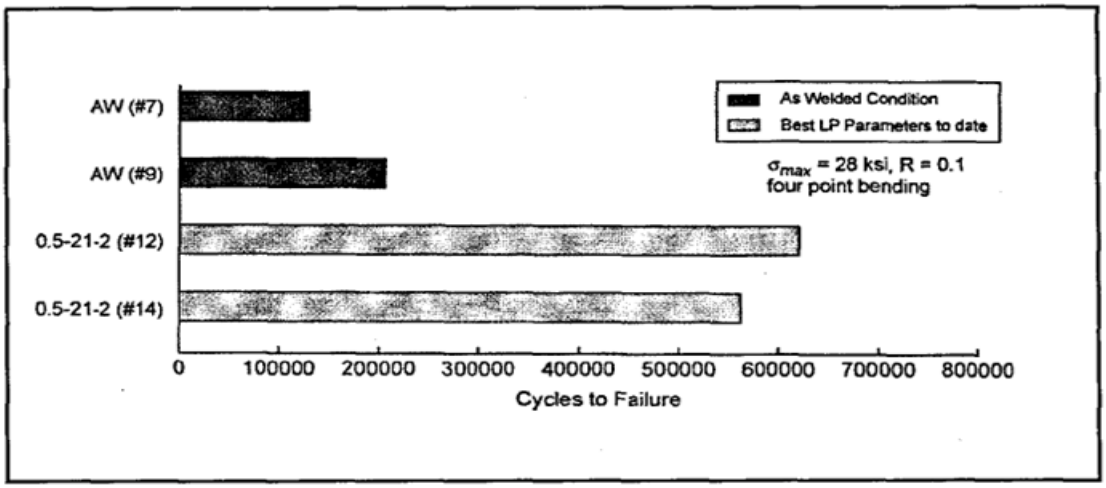

Figure 12. Four point bend fatigue results of laser peened and as welded aluminum 5059-H116. (From [4])

Hatamleh studied the SCC behavior of both shot and laser peened friction stir welded 2195 aluminum alloy joints [17]. The peening effects using a slow strain rate test in 3.5% NaCl solution and the laser peened samples demonstrated superior properties to the other samples (Table 1). The residual stresses were also analyzed as shown in Figure 13.

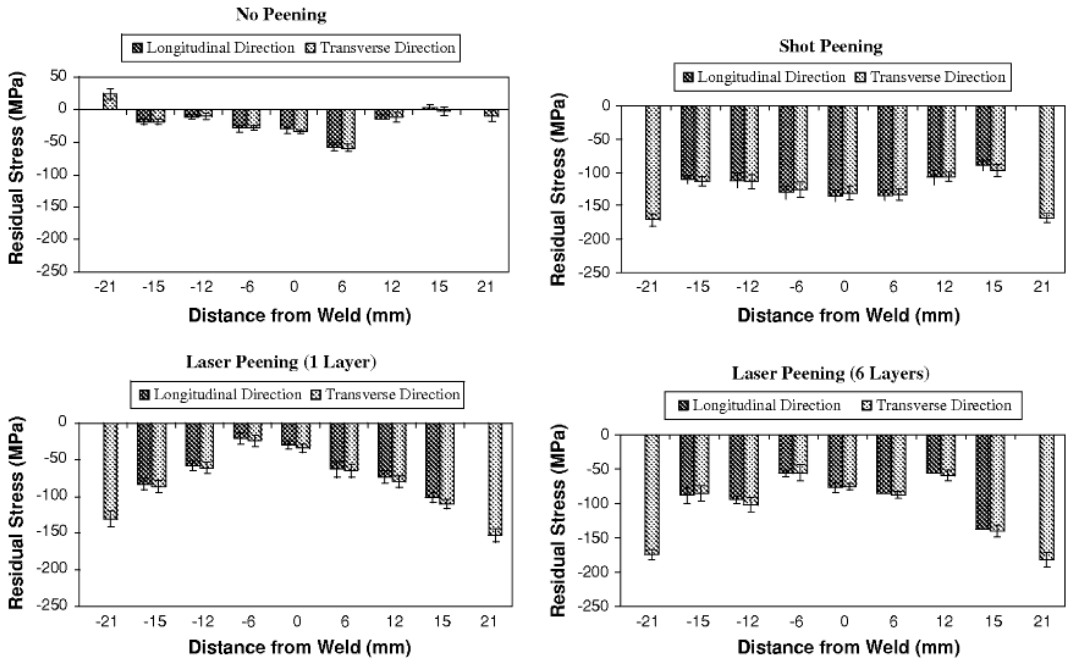

Figure 13. Residual stress for different peening conditions (From [13]).

Materials	Initial strain rate, s^{-1}	Ultimate tensile strength, MPa	% Area reduction	% Elongation	Stress corrosion cracking susceptibility
Laser peening (3 layers)	1×10^{-6}	432.2	18.37	4.10	No SCC
Laser peening (3 layers)	2×10^{-6}	440.0	12.99	4.01	No SCC
Laser peening (6 layers)	2×10^{-6}	444.2	10.64	3.01	No SCC
Shot peening	2×10^{-6}	423.0	13.68	4.27	No SCC
No peening	2×10^{-6}	423.5	15.30	5.27	No SCC

Table 1. Summary of slow strain rate test results for AA2195 tensile samples tested in 3.5% NaCl solution at room temperature (From [17]).

C. THESIS OBJECTIVES

The work in this thesis seeks to extend the application and the understanding of LP to stress corrosion crack mitigation in marine grade aluminum alloys. While research has been performed on the effects of LP on the fatigue life of 5xxx series aluminum alloys, the stress-corrosion effects have not been considered [4]. The effects of LP on

SCC have been considered on stainless steel Peyre [18]and on 2xxx series aluminum Hatamleh [17], but again, not on 5xxx series aluminum. Therefore, the first question investigated by this thesis is:

Does LP prevent SCC at fusion welds in AA5083?

Our hypothesis is that LP will help prevent SCC in fusion welds on AA5083. LP should generate large, compressive stresses that will lessen, or completely remove, the tensile stresses in the heat affected zone that drive SCC in these materials. The second question is:

How does LP alter the microstructure of the AA5083 material?

Our hypothesis is that LP will generate a large amount of plastic deformation in the microstructure. This plastic deformation will be manifested by a clear increase in hardness at the surface of the material and by a measurable increase in orientation spread within the aluminum grains themselves. We posit that both the plastic deformation and the resulting compressive stresses are important to the prevention of SCC in these materials.

II. EXPERIMENTAL PROCEDURE

A. MATERIAL PROCESSING

1. Plate Fabrication

The material used is the aluminum alloy 5083 with the heat treatment H116 (AA5083.) The chemical composition of AA5083 is: magnesium 4.7, manganese 0.9, iron 0.20, silicon 0.10, chromium 0.08, zinc 0.03, copper 0.03, titanium 0.01, and the remainder aluminum. The AA5083 composition was certified by the American Bureau of Shipping.

2. Welding

Three sheets of AA5083 were split in half parallel to the rolling direction. All cutting of the samples was done by a band saw with lubricant, in which no heat was added. The half sheets were then welded back together using a metal inert gas weld (MIG) at the Carderock Division, Naval Surface Warfare Center (NSWCCD) (Table 2). Each weld consisted of four beads, three on the front of the plate and one on the root of the weld (Figure 14).

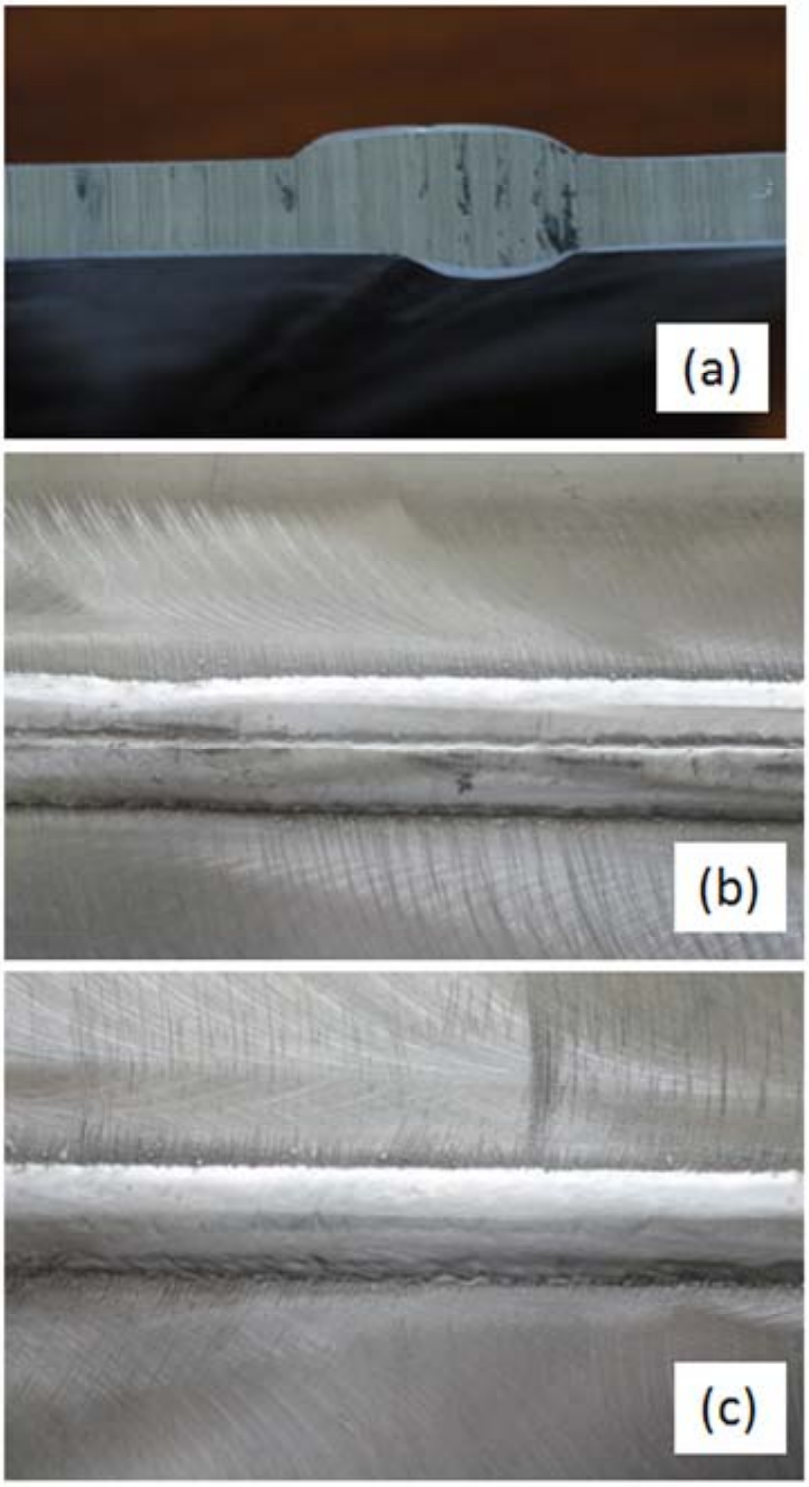

Figure 14. Welded Material (a) side view (b) top view and (c) side view.

Bead	Volts	Wire Feed	Amps	Travel Speed	Weld Time	Inter-pass Temp	Remarks
1	23.9	273	121	17.4	1:16	69.6	Plate 1
2	25.1	336	136	17.4	1:15	118.3	
3	25.5	336	134	17.4	1:15	138	
4	25.1	336	138	17.4	1:14	72.9	Bead on the back of plate
1	23.7	273	122	17.4	1:15	69.8	Plate 2
2	25.4	336	134	17.4	1:15	120.8	
3	25.5	336	133	17.4	1:14	170.5	
4	24.9	336	139	17.4	1:16	72.3	Bead on the back of the plate

Table 2. Weld procedure from Carderock Division, Naval Surface Warfare Center (CDNSWC) for sample welds used.

B. LASER PEENING

1. Process

All LP was completed by Metal Improvement Company (MIC) in Livermore, CA. The sample sheets were cut into sample strips of 2 inches in width for the slow strain rate testing (SSRT) and 6 inch squares for the potentiostat corrosion testing. The variables for the LP for the SSRT samples are displayed in Table 3 and for the potentiostat corrosion testing in Table 4. The conditions for the SSRT specimens were chosen in order to perform a statistical effects analysis with a full factorial design of three factors and two levels. No tape was used on the surfaces of the samples to be peened. LP can be performed with or without tape on the surface and the differences in the LP effect appear to be slight [14]. Because of our interest in applying LP to large-scale, ship structures, we decided to forego the taping of surfaces to be peened.

Sample Designator	Irradiance (GW/cm^2)	Pulse Width (ns)	Layers (full coverage)
F	1	18	1
G	1	18	2
H	3	18	1
I	3	18	2
J	1	27	1
K	1	27	2
L	3	27	1
M	3	27	2

Table 3. Laser peening conditions for SSRT samples. Provided by MIC.

Sample Designator	Irradiance (GW/cm^2)	Pulse Width (ns)	Layers (full coverage)
I	1	18	1
II	3	18	1
III	3	27	2

Table 4. Laser peening conditions for potentiostat experiment. Provided by MIC.

C. SLOW STRAIN-RATE TESTING (SSRT)

1. Sample Preparation

Specimens for slow strain-rate testing were fabricated from the welded plates described above according using similar geometries of that used in the work of Zucchi et al. and Ogoucha et al. [9, 10]. The relevant dimensions are shown in Figure 15.

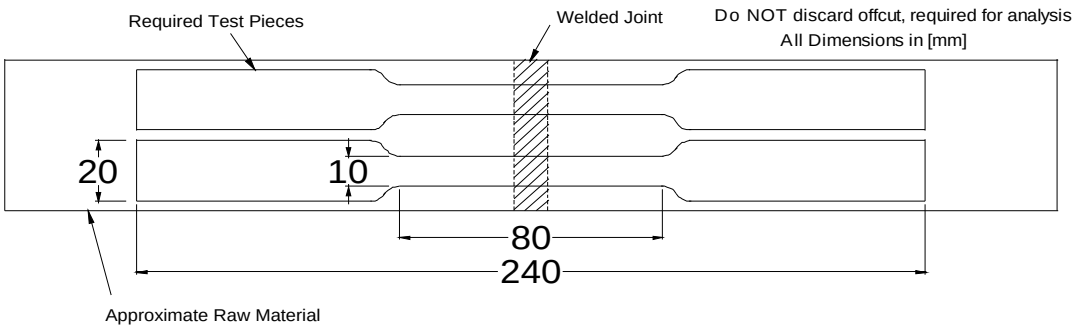

Figure 15. SSRT samples dimensions. All dimensions are in millimeters.

Laser peening was performed prior to machining test samples. The machining was performed at the NPS MAE machine shop using a modified end-mill with a large volume of coolant flow to prevent sensitization or microstructural evolution during machining. All samples were cool to the touch immediately after machining. The sample edges were manually de-burred with a file after machining. The as-machined surface finish was deemed satisfactory for SSRT.

Additional SSRT control samples were fabricated from the same plate stock but without welds. The same sample geometry and fabrication techniques were used for this material as described in Figure 15. One set of samples was simply extracted from the 5083 H116 plate without further modification. Another set of samples was intentionally sensitized by placing in a furnace at 175°C for 168 hours using conditions based upon the work of Ogoucha et al. [10].

The corrosive solution for the SSRT was based upon the work of Ogoucha et al. [10] and consisted of distilled water as a solvent with 3.5wt% NaCl and 0.3wt% H_2O_2 added. The hydrogen peroxide was added to the solution to increase the oxidation potential that drives SCC. To prevent SCC from initiating on the un-peened edges of the samples, the edges were coated with Gesswein Stop-Off Lacquer.

A special sample holder was designed for this work to allow intimate contact of the SSRT specimen with the corrosive solution during testing while allowing unconstrained displacement of the load frame (Figure 16).

Figure 16. SSRT sample from top: initial securing puck, with Tygon tubing, and with silicone.

The specimens can strain as much as twenty percent during these tests, so the unconstrained displacement requirement is essential. The sample holder geometry consisted of pushing the grip section of an SSRT specimen through a mold and then filling the 1 ¼" mold with Buehler Sampl-Kwick two-part epoxy. Once the epoxy had set, the sample was removed from the mold. A Tygon tube, with a 1 ¼" inner diameter, was then fitted over the epoxy cylinder. This tube served as the container for the corrosive solution and was 11 mm in length, which is long enough to allow for the entire gage section of the SSRT specimen to be immersed during testing. To prevent leaking of the corrosive solution, silicone caulk was placed around the outside bottom of the specimen. The silicone was allowed to cure for 24 hours prior to testing.

2. Slow Strain Rate Testing

The SSRT was carried out on an Instron 4507 test frame (Figures 17 and 18). This instrument used an Instron load cell with a load rating of 200 kN static and 100 kN dynamic in both compression and tension, for force measurement and screw-driven, cross-head displacement for strain measurement. The 4507 frame has a testing speed range of 0.001 to 500 mm/min. All stresses and strains were computed as engineering stresses and strains using the original and final dimensions of the specimen. As these tests were concerned primarily with strain to failure, these measurements of stress and strain were deemed sufficient. All tests were performed with a constant extension rate of 50 nm/second. This displacement rate was chosen based upon a desired uniaxial strain rate of 10^{-6} for the geometry of specimen shown in Figure 15. This strain rate is consistent with the work done by Zucchi and Hatamleh [5, 13]. It is also within the parameters set forth in ASTM G 129-00, Standard Practice for Slow Strain Rate Testing to Evaluate the Susceptibility of Metallic Materials to Environmentally Assisted Cracking [19]. It should be noted that this displacement rate only gives a strain rate of 10^{-6} at the start of the test. The strain rate decreases as the specimen becomes longer.

Figure 17. Instron 4507 test frame used in the SSRT testing of laser peened samples.

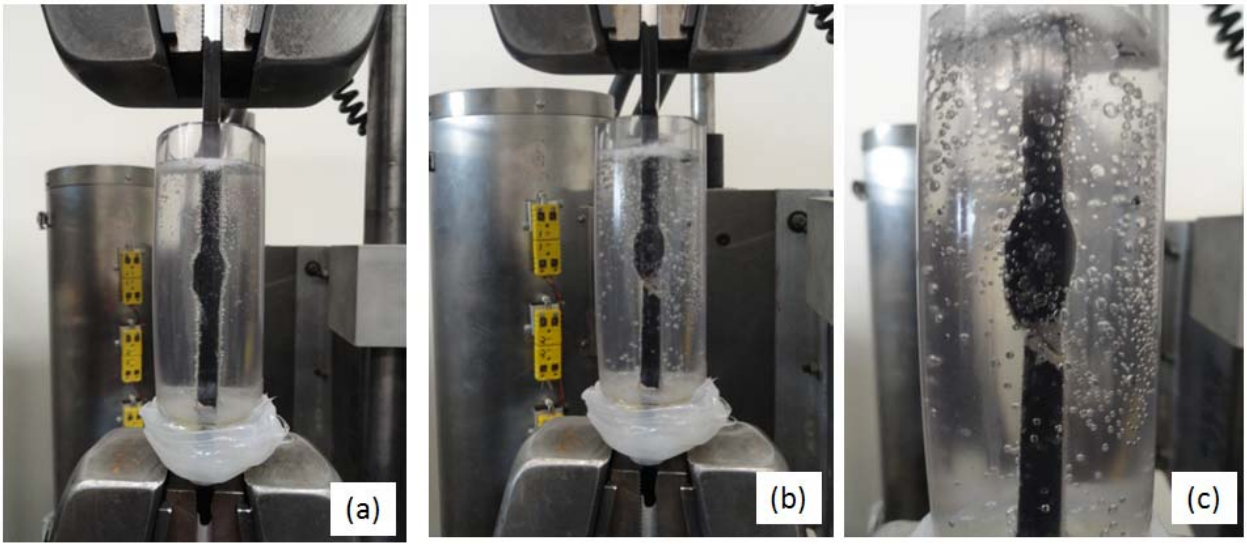

Figure 18. Sample in Instron (a) unbroken (b) broken and (c) close-up.

D. POTENTIAL-DRIVEN STRESS CORROSION CRACKING

1. Sample Preparation

Given the important relationship between electrochemical potential, and the initiation of SCC, experiments were performed with welded AA5083 plates, with the potential carefully controlled relative to a Ag/AgCl reference electrode with a standard adder potentiostat. This test was done to accurately determine the electrochemical conditions that drive SCC. These experiments were performed on control welded plate as well as on the LP 1-18-1 plate.

Plates 2 inches wide and 6 inches long were machined from master welded plates that had been laser peened on both sides using the conditions above. Holes (1/4" diameter) were tapped to receive the working electrode described below. No further processing was performed on these plates. The edges of all sides were coated with Gesswein “Stop-Off” Lacquer to prevent SCC on the sides of the plate. The sides of the plate were not laser peened.

2. Potentiostat Set-Up

The potentiostat experiment was set up using a commercial potentiostat controller, Gamry Instruments (series G300 Potentiostat), in a specially designed

configuration (see Figure 19). The working electrode in all cases was the aluminum plate in which we attempted to drive SCC. Electrical contact was made through a 316 stainless steel threaded rod screwed into the plate. The junction between this rod and the plate was sealed using silicone caulk. A simple graphite rod provided the counter electrode. The reference electrode was an Accumet Materials Co. Ag/AgCl standard reference cell. The samples were housed in an 8" x 6" Pyrex baking dish. The corrosive solution was distilled water with 3.5 weight percent NaCl added. No hydrogen peroxide was added to this solution, in that a set potential was being used to drive corrosion. Two samples were tested simultaneously by linking them as working electrodes. No specific controls were used for atmosphere or temperature. A Top Fin Air Pump 1000 and Ceramic Airstone was use to maintain the oxygen level with in the dish and a pH meter was put in place to ensure that the solution did not become overly acidic (pH<4).

The potentiostatic experiments were preceded by a cyclic polarization curve. This measurement was necessary to determine the appropriate potential to apply for inducing stress corrosion cracking. Too high of an applied potential will simply result in anodic dissolution of the sample, not stress corrosion cracking. The potentials for the potentiostatic experiments in this thesis were chosen to be in the passivation region for the material to allow for the formation of a passive layer, hypothesizing that film rupture would be the primary mechanism for stress corrosion cracking. The cyclic polarization curve was made from -1V to +1.5V with respect to the open circuit potential. An initial delay of 60 seconds was used with a scan rate of 1 mV/second for both the forward and reverse curves.

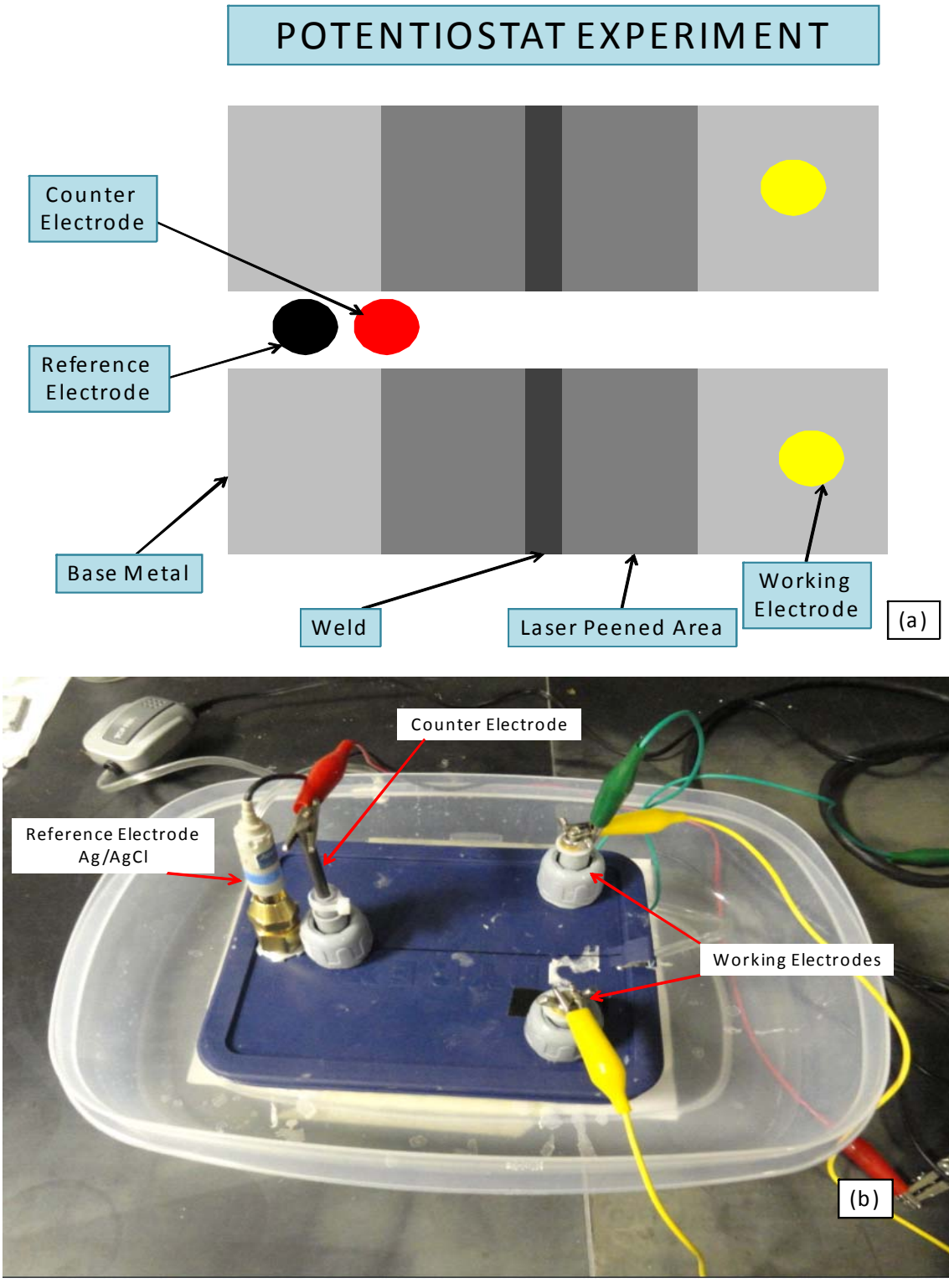

Figure 19. Design for potentiostat experiment. (a) Schematic showing design of potentiostat experiment. (b) Photograph of experimental configuration.

E. MICROSTRUCTURAL ANALYSIS

1. Metallographic Sample Preparation

The 1" samples were cut using the Buehler Isomet 200 precision saw and mounted in Buehler Sampl-Kwick two-part epoxy in a 1 ¼" puck form. The samples were metallographically prepared in a standard fashion using a number of steps (Table 5). The first step was to grind the sample pucks using a Buehler Ecomet 4 Variable Speed Grinder-Polisher. The sample surface was ground using a succession of finer grit silicon carbide sandpapers, starting with 320 grit and completing with 4000 grit. Each grit was applied to the sample surface in 3 rounds of 5 minutes at 140 rpm. Between each grit level, the sample was rinsed well with water and then methanol.

Next, the samples were polished using a Buehler Ecomet 3 Variable Speed Grinder-Polisher. This process was completed in three steps. First, a 3μm Buehler MetaDi monocrystalline diamond suspension solution was used for 3 rounds for 5 minutes each at 120 rpm. Next, a 1μm Buehler MetaDi monocrystalline diamond suspension solution was used for 3 rounds for 5 minutes each at 120 rpm. Finally, a 0.05μm Buehler Mastermet Colloidal Silica Polishing Suspension solution was used for 3 rounds for 5 minutes each at 120 rpm. Between each step, the samples were rinsed well with water and then methanol. Upon completion, the samples were ultrasonically cleaned using a Buehler Ultramet 2005 Sonic Clearer for 5 minutes in methanol and then dried with a hot air gun.

After competition of the basic metallography, the samples were finished either by electropolishing or vibratory polishing. The samples were electropolished in a Buehler Electromet 4 Electropolisher using a solution of perchloric acid at 0ºC. The vibropolishing was completed using a Buehler Vibromet 2 Vibratory Polisher with a 0.05μm MasterMet Colloidal Silica Polishing Suspension solution. After both process the samples were rinsed thoroughly with methanol and dried with a hot air gun.

STEP	PROCESS	TIME	RPM
1	320 Grit SiC Paper	15	140
2	600 Grit SiC Paper	15	140
3	2400 Grit SiC Paper	15	140
4	400 Grit SiC Paper	15	140
5	3 Micron MetaDi Diamond Suspension	15	120
6	1 Micron Metadia Diamond Suspension	15	120
7	0.05 Micron Colloidal Silica	15	120

Table 5. Grind and Polishing Conditions

2. Fracture Surface Characterization

The fracture surfaces of the broken SSRT samples were characterized to determine the nature of the fracture, ductile versus brittle, and to determine the length of the pre-crack for each fracture condition. The fractured SSRT samples were cut on the side closest to the weld so that each one could fit into a circular sample holder designed to hold 12 samples (See Figure 20.) The holder was mounted on a pedestal in the Zeiss NEON 40 field emission gun scanning electron microscope (FEG-SEM) and placed into the vacuum chamber with the door closed. The fracture surface of each SSRT sample was then examined at the following magnifications: x23, x150, x500, and x2000. At x23 the pre-crack length was measured as the distance from the surface of the sample to the edge of the fracture. The measured length was corrected for the approximately 45 degree tilt of the surface with respect to the image to calculate the true pre-crack length on the fracture surface itself.

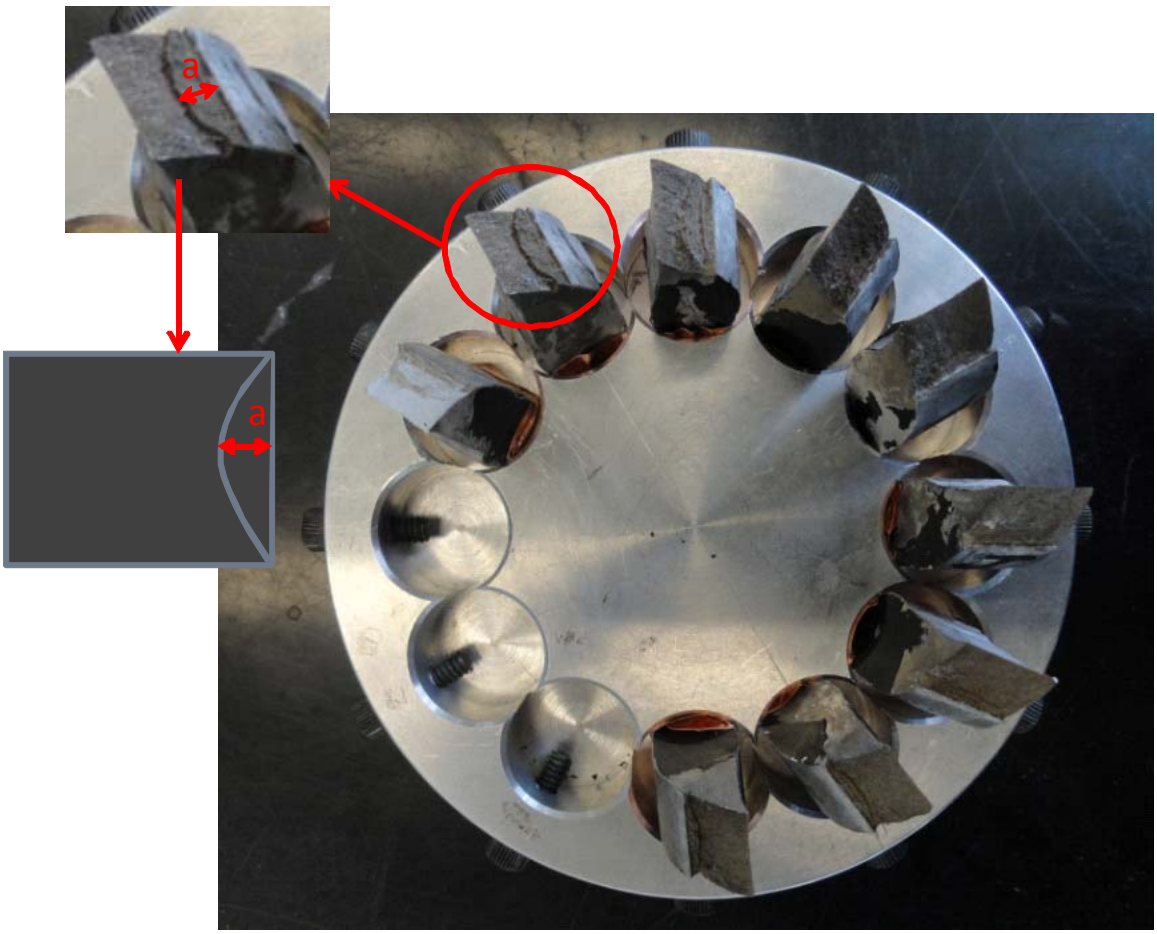

Figure 20. Mount for broken SSRT samples for use in SEM with close up of fracture surface indicating critical crack length (a).

F. HARDNESS MEASUREMENTS

1. Hardness Tests

Hardness measurements were made to investigate the effects of LP on the hardness, and by proportion, on the yield strength of the aluminum microstructure. Rockwell hardness was used to measure the change in hardness in the base material as a function of laser peening. Vickers microhardness was used to measure the changes in hardness as a function of position across welds.

2. Rockwell Hardness Measurements

Rockwell hardness measurements were made on the base metal region of the laser peened specimens and on control 5083. These measurements were made on the as-peened surface of tensile bars after SSRT testing between the start of the grip section into the gage section. The hardness measurements were made on the Rockwell B scale using 100kg load with a 16mm steel ball as the indenter. A Rockwell B standard of 58.7 was used prior to the measurements to check the calibration of the instrument. Five hardness tests were performed for each sample with the exception of the control and the 3-27-3 sample which each received ten tests.

3. Vickers Microhardness Measurements

Vickers microhardness measurements were made using a HVS-1000 Digital Microhardness Tester. For the hardness profiles across welds, a load of 3N and a hold time of 10 seconds were used for each indentation. A diamond, Vickers indenter was used to make the indentations. Indentations were spaced by 500μm, approximately six times their width.

THIS PAGE INTENTIONALLY LEFT BLANK

III. RESULTS AND DISCUSSION

A. SSRT FRACTURE AND ANALYSIS

1. SSRT Results

The results of the non-welded, control samples in a solution of distilled water as a solvent with 3.5wt% NaCl and 0.3wt% H_2O_2 and air; and non-welded sensitized (168 hrs at 175ºC) in the same solution and air are shown in Table 6. Both the control sample and the sensitized sample in air showed fairly consistent results with only a slightly higher strain to failure for the sensitized-in-air sample, most likely due to the increased ductility of the metal once the magnesium was removed from solid solution [10]. All three samples also fractured at a 45º angle, indicating that the failure was driven by plane-stress, ductile fracture. The sensitized sample in solution showed the expected, drastic decrease in both strain to failure and maximum stress as shown in Figure 21. In addition, it did not break at a 45º angle but had relatively flat fracture plane with a jagged fracture path, indicative of a brittle fracture caused by SCC.

Sample	Process	Test Medium	Strain at Failure (%)	Max Stress (MPa)
A	Control	Air	14.98	303.25
B	Control	Solution	16.74	394.51
C	Sensitized	Air	18.08	304.96
D	Sensitized	Solution	4.94	249.09

Table 6. SSRT Results for Non-Welded Control and Sensitized Material.

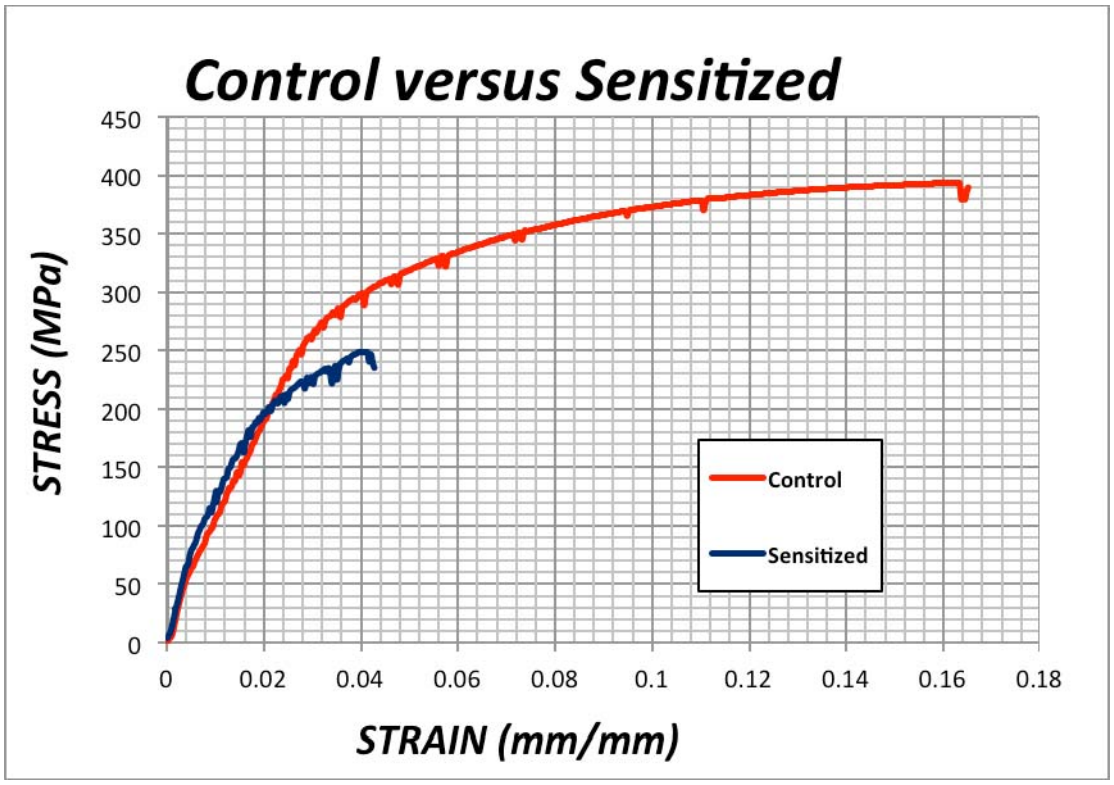

Figure 21. Control versus Sensitized stress strain curve.

The results of the SSRT tests for the welded samples, both control and laser peened are shown in Table 7. Figure 22 shows the stress strain curve for samples E, F, H, and M which correspond to the control sample, LP 1-18-1, LP 3-18-1, and LP 3-27-2. The aforementioned samples were chosen as a representative sample and display the full range of laser peened intensity starting with the lightest (LP 1-18-1) to the most intense (LP-3-27-2). The LP 3-27-2 had the lowest strain to failure and as the intensity of the laser peening decreased the strain to failure increased.

The serrations seen on the stress strain curves have been investigates by Wen, et al. Al-Mg alloys often exhibit serrated yielding when deformed at room temperature. It is caused by solute atoms forming atmospheres around the dislocations. The dislocations then have to break away from the atmosphere before they can continue their motion creating the serrations seen on the curves [20].

Sample		Laser Power	Pulse Duration	# Layers	Test Medium	Strain at Failure	Max Stress
E	*				Solution	9.28	308.32
E Control					Air	7.27	202.56
F	*	1	18	1	Solution	9.81	331.91
G		1	18	2	Solution	8.25	310.55
H	*	3	18	1	Solution	8.42	322.34
I		3	18	2	Solution	6.91	199.49
J		1	27	1	Solution	8.34	225.94
K		1	27	2	Solution	6.74	212.36
L		3	27	1	Solution	6.7	212.75
M	*	3	27	2	Solution	6.54	318.58

Table 7. Results for welded controlled and laser peened samples.

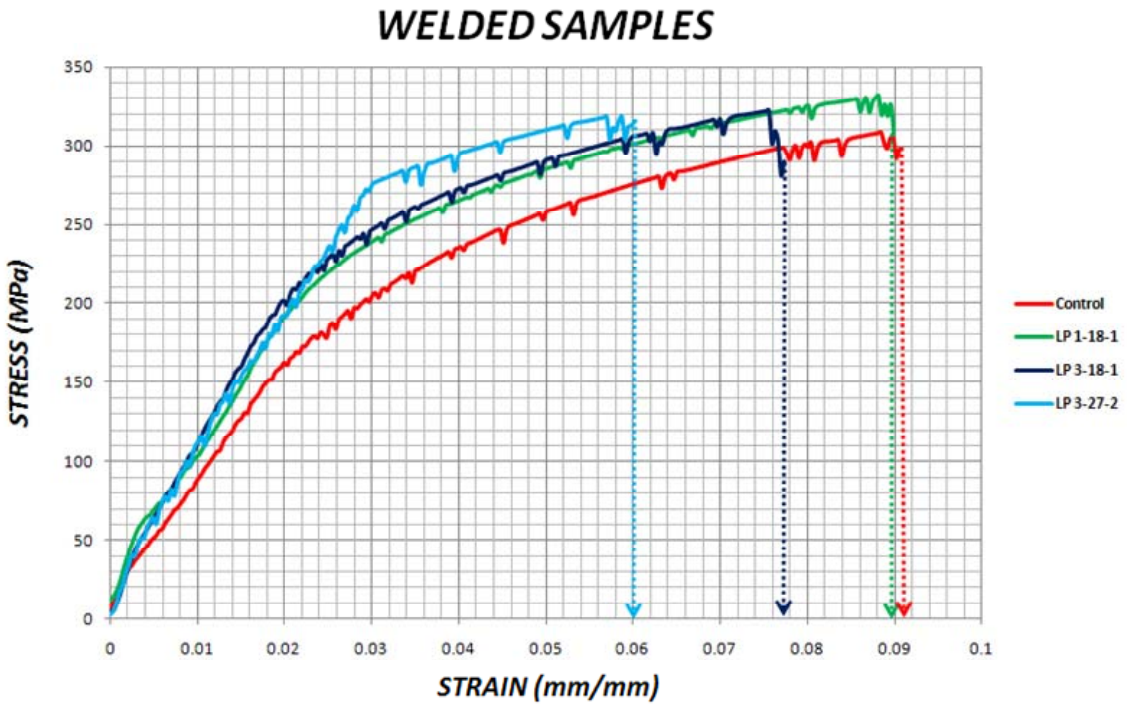

Figure 22. Welded samples stress strain curve.

The analysis of variance (ANOVA) approach was used to assess statistical significance of LP parameters (Table 8) [21]. The independent variables used were strain-to-failure and maximum stress. The dependent variables used were laser power density (GW/cm^2), pulse duration (ns), number of layers of peening and their interactions. None of the parameters had a statistically significant effect upon the maximum stress. There was a clear statistical effect for all of the parameters on strain-to-failure, but none of their interactions had any significance. All of the primary factors had a negative impact on strain to failure but the largest effect is the number of layers.

Term	Estimate	Standard Error	t-Ratio	Probability>|t|
Intercept	13.8	1.01	13.7	0.0002
Laser Power	-0.571	0.161	-3.54	0.0240
Pulse Duration	-0.141	0.036	-3.93	0.0171
# of Layers	-1.21	0.323	-3.74	0.0201

Table 8. ANOVA results comparing strain to failure and laser peening factors on laser peened welded samples.

2. Fracture Surface Analysis

The microstructures of the SSRT fracture surfaces were examined using the SEM. The distance from the beginning to the end of the initial fracture lip was measured at 23x magnification to determine the pre-crack length as shown in Figure 23. The results are in Table 9. SEM images for samples F (LP 1-18-1), H (LP 3-18-1), and M (LP 3-27-2) are displayed in Figure 23. In the tests performed for this thesis, all laser peened samples exhibited ductile fracture surfaces as indicated by the dimpled appearance of the fracture surfaces as seen in Figure 24.

Sample		Laser Power	Pulse Duration	# Layers	Test Medium	a (mm)
E	*				Solution	2.79
F	*	1	18	1	Solution	2.412
G		1	18	2	Solution	2.591
H	*	3	18	1	Solution	1.798
I		3	18	2	Solution	1.325
J		1	27	1	Solution	0.7352
K		1	27	2	Solution	1.365
L		3	27	1	Solution	1.445
M	*	3	27	2	Solution	1.275

Table 9. Results for crack lengths of welded laser peened samples.

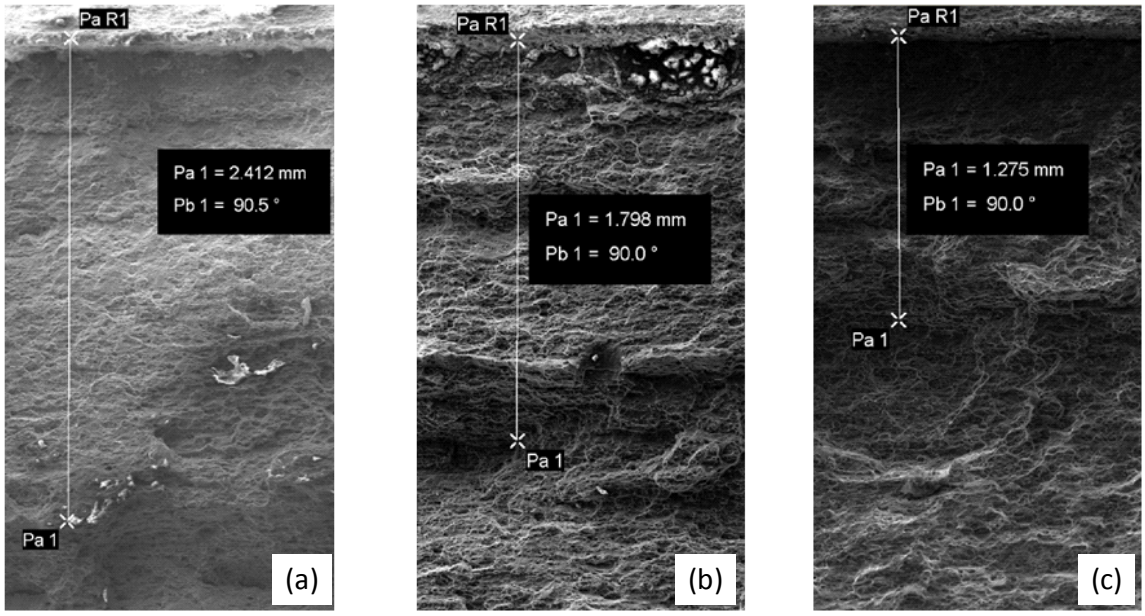

Figure 23. SEM images showing crack lengths for (a) F: LP 1-18-1 (b) H: LP 3-18-1 and (c) M: LP 3-27-2.

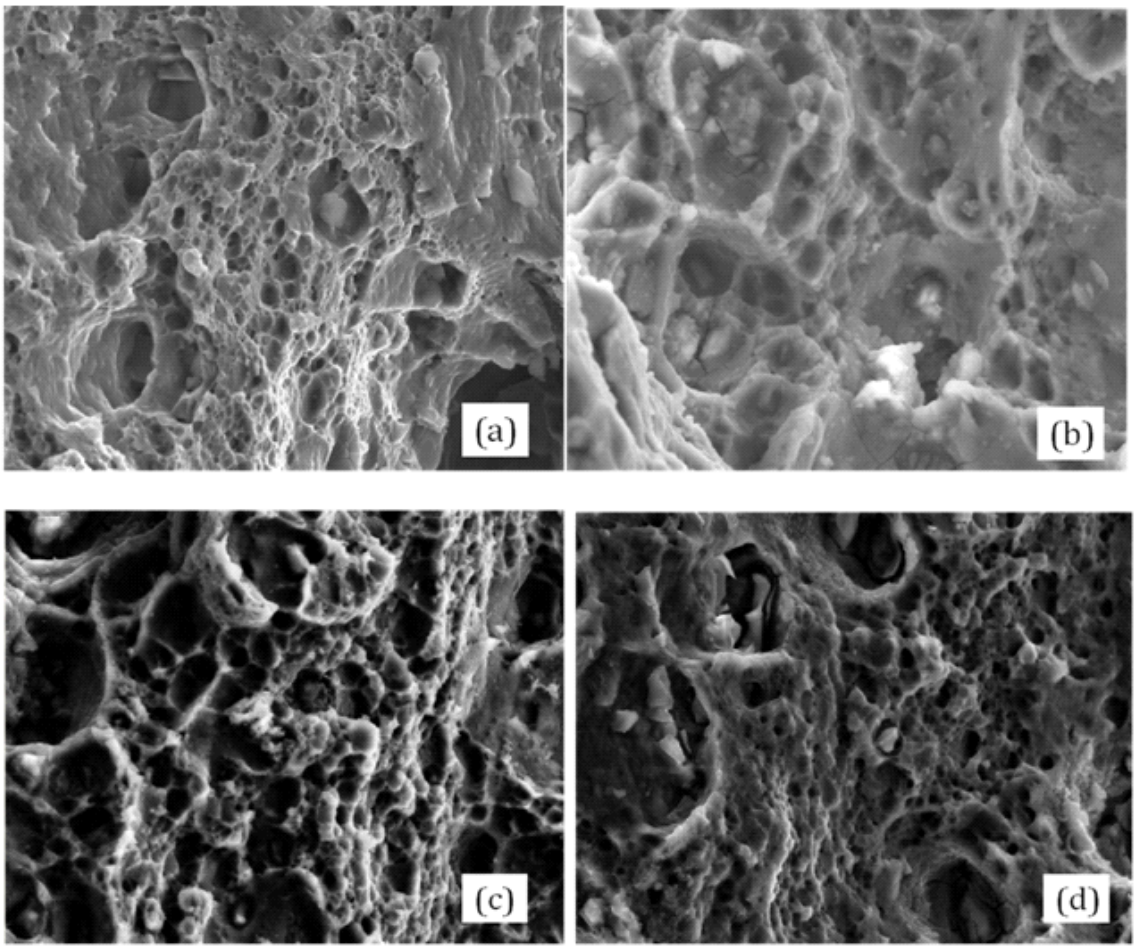

Figure 24. SEM at x500 for (a) Control Weld (b) LP 1-18-1 (c) LP 3-18-1 and (d) LP 3-27-2.

It is well known that the mechanism of crack propagation during SCC involves the periodic rupture of a brittle film formed at the crack root between crack extension events. In cases where SSRT is used to study crack extension in corrosive environments, and where ductile rupture persists, a slower strain may be required during testing, thereby providing the crack tip more time for repassivation between crack-extension events. While the chosen strain rate of 1×10^{-6} per second was based upon the published literature, clear evidence of SCC on the fracture surfaces was not observed. It is possible that the strain rate was not slow enough to enable such brittle film formation to occur, which is a necessary condition for SCC. It is therefore recommended that even slower strain rates

be considered in the future. Another possibility is that the carefully controlled welding process employed by the welders at NSWCCD did not sufficiently sensitize the weld and HAZ to promoted stress corrosion cracking.

3. Fracture Analysis

Using the fracture mechanics model, $K_c = Y * \sigma * \sqrt{a_c}$, the fracture toughness, K_c was calculated (Table 10). Y is our assumed geometry factor, which is assumed to be approximately constant for all the cases. We used the maximum stress value for σ and the measured pre-crack lengths for the critical flaw sizes, a_c. A general trend was found that the more intense the laser peening, the lower the K_c value indicating a more brittle sample area as can be seen in Figure 24.

Sample	a (mm)	Kc ($Mpa\,m^{1/2}$)
LP 1-18-1	2.412	28.8924
LP 1-18-2	2.591	14.5689
LP 3-18-1	1.798	24.2261
LP 3-18-2	1.325	12.8707
LP 1-27-1	0.7352	10.8585
LP 1-27-2	1.365	13.9064
LP 3-27-1	1.445	14.3344
LP 3-27-2	1.275	20.1627

Table 10. Fracture Toughness (K_c) values for laser peened SSRT samples.

4. Comparsion With Literature

Searles, et al. investigated stress corrosion cracking of sensitized AA5083. [22] Figure 25 show their results for constant extension rate tests (CERTs) for a control sample and a sample that had been sensitized for 189 hours at 150ºC with a -0.980 V polarization. Their results are comparable to those found and displayed on Figure 21.

Searles found a trend showing that the amount of ductility in a material is inversely proportional to the amount of β phase present in the material. He found that the amount of β continued to increase in the material the longer it was sensitized up to 189 hours at 150ºC and then was followed by a slight recovery at longer sensitization times as shown in Figure 26. Figure 26 also shows how the β phase precipitates continue to migrate to grain boundaries with an increase of sensitization time. Searles also found that even after a sensitization time of 262 hours the sensitized conditions did not have a great enough effect to alter the mechanical properties of the material, in agreement with our results from Table 7. Both finds are further evidence of the necessity that all three of the requirements for SCC are needed to reduce the effectiveness of the material. Sensitized AA5083 in a non-corrosive environment will be able to perform with the standard material properties but if the material is placed in a corrosive environment then the integrity of the material will be greatly reduced.

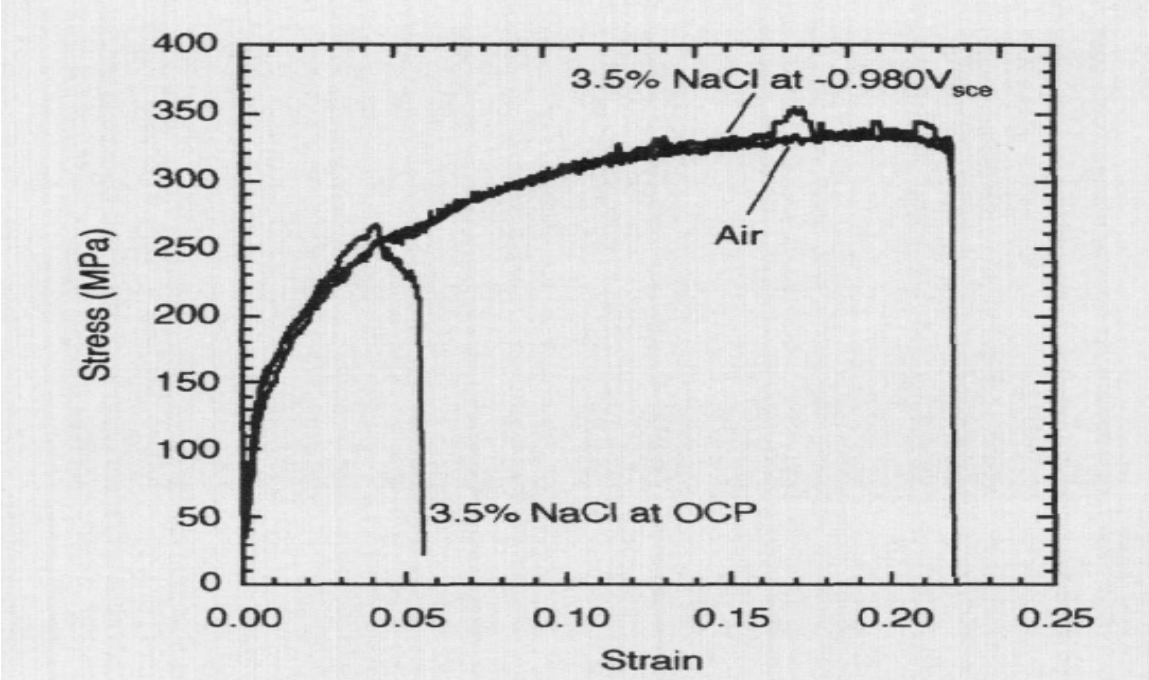

Figure 25. CERT data for 189 h sample showing ductility recovered at -0.980 V polarization during testing (From [22]).

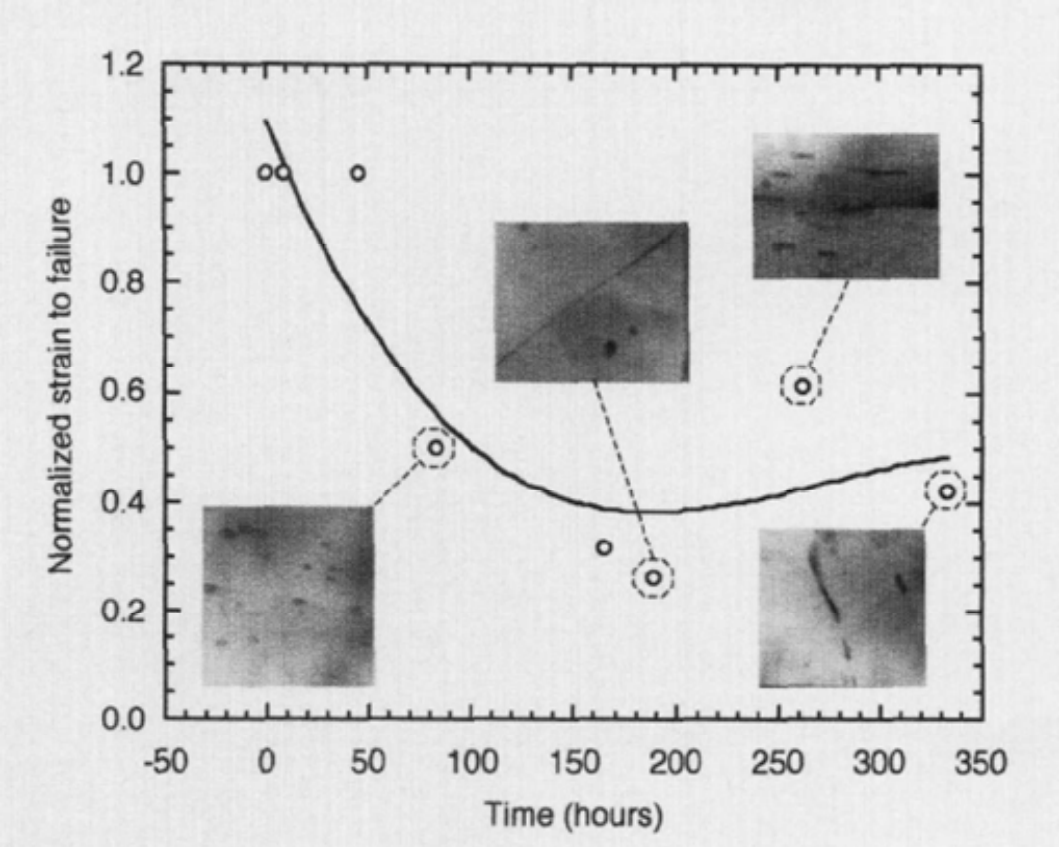

Figure 26. Normalized strain to failure vs. sensitization time. Insets show TEM micrographs of the degree of grain-boundary precipitation at selected times (From [22]).

Hatamleh found similar results in his SSRT testing in his work with 2195 aluminum alloys joints as seen in Table 1 [17]. The strain to failure also decreased with increased shot and laser peening levels as observed here. They note that the ultimate tensile strength increases with increased peening, but no ultimate tensile strength is observed from the stress-strain curves in their mechanical test data, and it must be assumed that they are equating the maximum stress with the ultimate tensile strength.

B. LP EFFECTS ON HARDNESS

1. Hardness Results

Rockwell B hardness measurements were made on the laser peened base metal. All LP conditions (samples F-M) have a higher hardness than unpeened material (sample

E) as seen in Figure 27. Only laser power, or irradiance (GW/cm^2), has a significant ($t=2.63$, $p<0.05$) effect when describing the variance in hardness. Hardness increases with increasing irradiance.

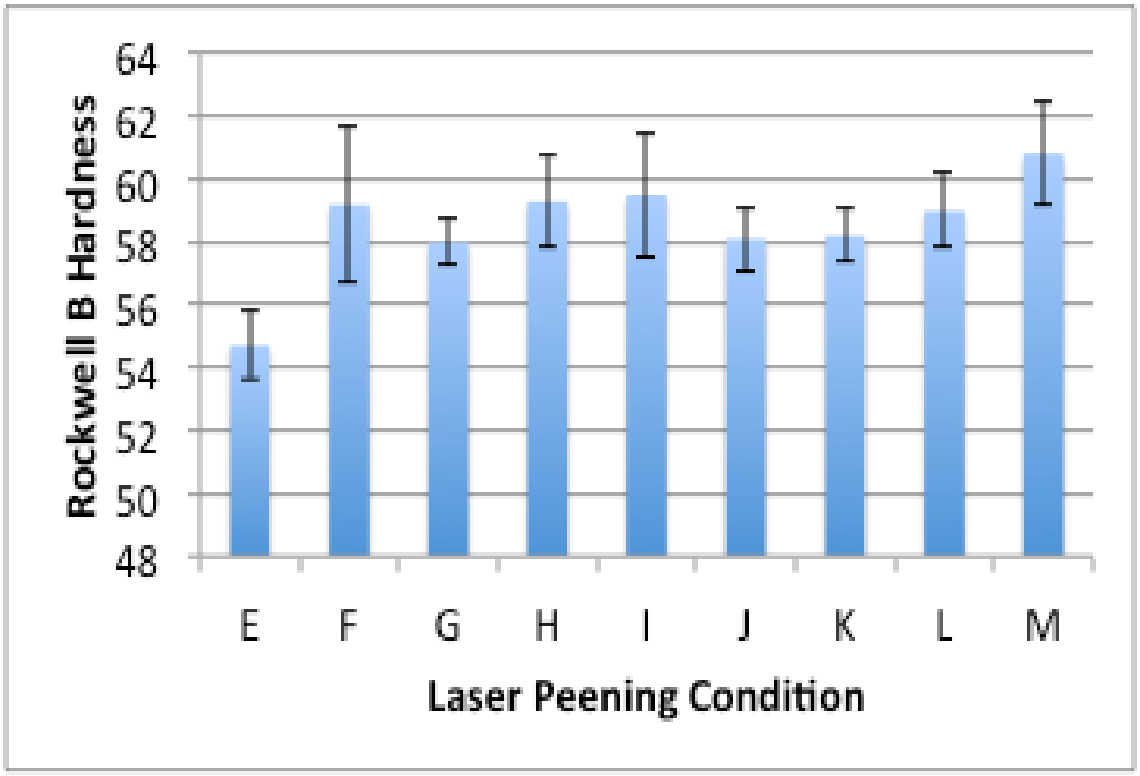

Figure 27. Rockwell B hardness data on base metal on unpeened material (sample E) and peened material (sample F-M).

The microhardness data was then gathered across the weld through the HAZ into the base metal using the Vickers Hardness test. Figure 28 compares the microhardness data and the most intense laser peened condition, LP 3-27-2. The control weld displayed a typical hardness profile with a softer area in the weld and into the HAZ. There is only slight increase in hardness in the base metal but a qualitatively large difference in hardness in the welded region and the HAZ. LP appears to even out the hardness profile of the HAZ into the weld, making a more uniform hardness profile throughout the sample.

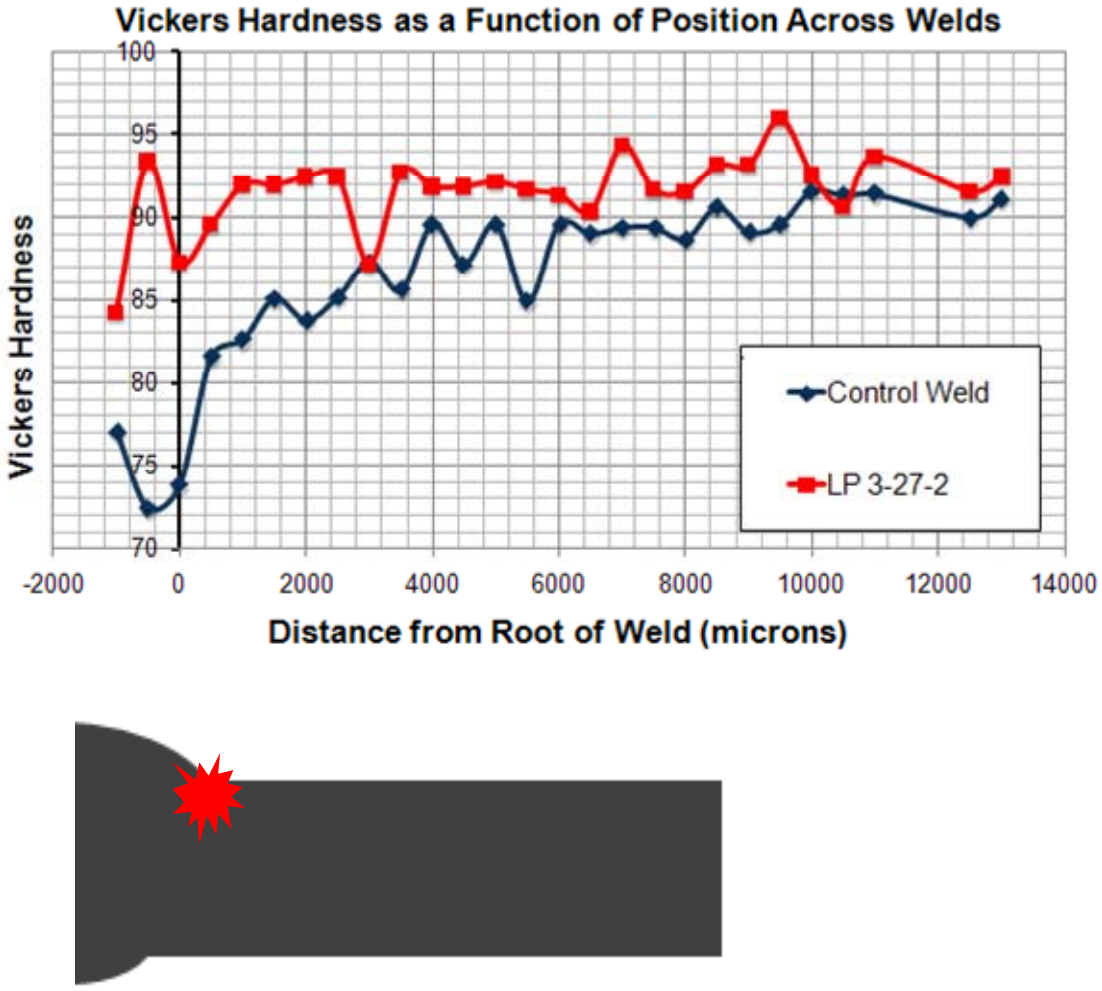

Figure 28. Vickers hardness as a function of position across the weld for the control weld and LP 3-27-2. The red indicator on the below diagram (the base of the HAZ) aligns with the 0 point on the distance axis.

2. Effects of Hardness on Fracture Response

As discussed above, a simplistic model for fracture in these experiments suggests that the plane stress fracture toughness (K_c) may be reduced by LP. In addition, we have observed that the hardness of the HAZ and weld portions of the tensile bar can be increased by LP. A possible connection exists between these observations. The K_{IC} of metals is generally inversely proportional to the yield strength of the material [23]. The yield strength of metals varies proportionately with hardness. For metals with limited strain hardening, the yield strength is often estimated as one third of the hardness [24]. It

is therefore likely that the observed increases in hardness at the HAZ-weld portion of the material correspond to a locally increased yield strength, which in turn, is reducing the K_C value of the material. The real situation is more complex as there should be a sizeable compressive residual stress interacting with the crack nucleation and propagation in the near and sub-surface areas at the weld.

C. POTENTIAL-DRIVEN STRESS CORROSION CRACKING

The cyclic polarization curve measured in the potentiostat described in the Experimental Methods section resulted in a result typical for AA5083 (Figure 29). The corrosion potential, E_{corr}, was measured to be approximately -1.1V. A clear passivation region was exhibited as the potential was increased from -1.1V to approximately -0.7V. Further increase in voltage displayed active corrosion. Upon potential reversal at +0.2V, a hysteresis was observed in the curve due to repassivation. The repassivation potential, $E_{repassivation}$, was measured to be approximately -0.8V.

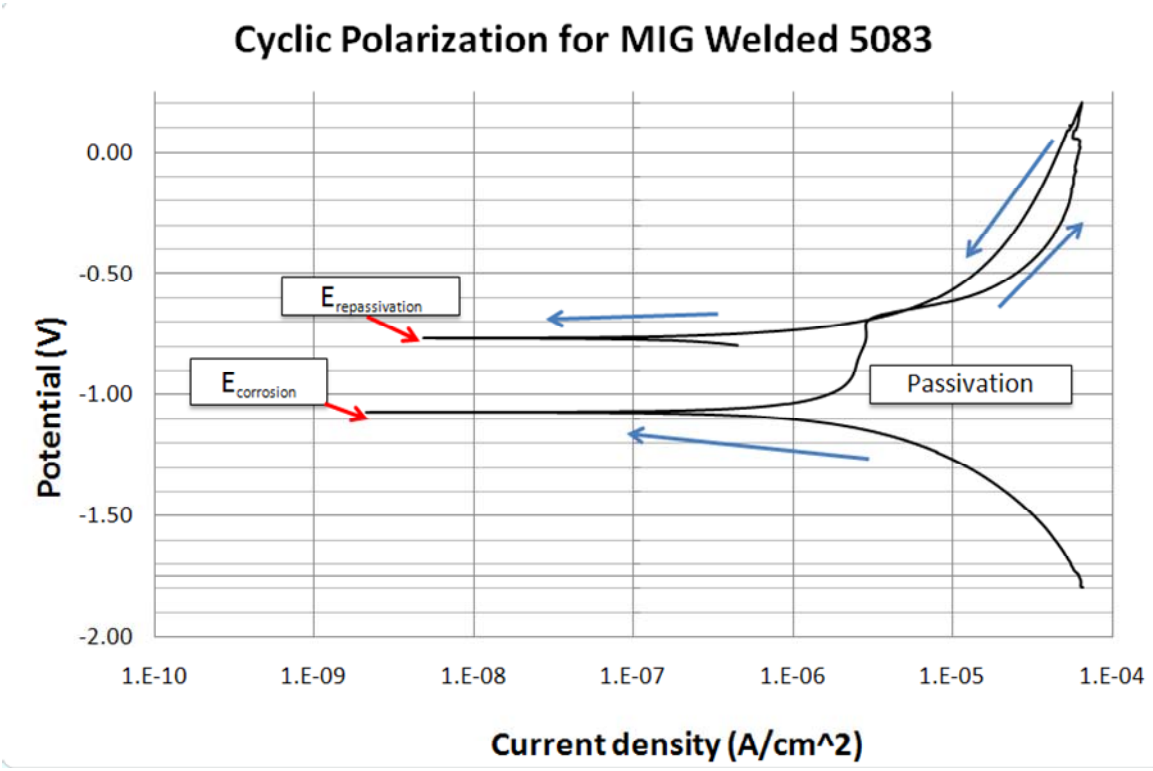

Figure 29. Polarization curve from combine control weld and 1-18-1 laser peened sample using custom-designed potentiostat described in Figure 30.

The potentiostatic responses of the control weld and the 1-18-1 laser peened weld were measured as a function of time for more than $2.3*10^6$ seconds total. The applied potential was selected to be in the passivation region for the material based upon the measured repassivation potential (Figure 30). Individual potentiostatic tests were run for times between $3*10^5$ and $8*10^5$ seconds. An example of such a test is shown in Figure 30, which shows the constant potential at -0.65V with time varying current density. The current fluctuated between 2-6$\mu A/cm^2$. After such times, the test was interrupted, the samples were removed from the potentiostat, and the welds were carefully inspected, under an optical microscope, for stress corrosion cracks. No stress corrosion cracks were observed after any segment of the potentiostatic testing.

The lack of stress corrosion cracking in these measurements is unexpected and may point to an overestimate of the amount of sensitization during MIG welding of AA5083. The lack of SCC in the potentiostatic measurements is either because there was not enough residual stress in the welds or because of a lack of sensitization from the heat of the welding process. Although the residual stress levels have not yet been measured for the welds in this thesis, the work of James et al. (Figure 4) suggests that it is unlikely that a lack of tensile residual stress explains the absence of SCC [7]. The more likely reason is the heat input during welding was not enough to achieve the critical level of sensitization necessary for SCC. The work of Zucchi et al. attributes the reduction in strain to failure of MIG welds in AA5083 to SCC, but they also note that this loss in ductility is partially from porosity in the weld [9]. In addition, the micrographs of the fracture surfaces are more indicative of ductile fracture, not SCC. It may be that MIG welds in AA5083 are not as sensitive to SCC as assumed. Further work that varies the heat input during MIG welding should be performed to clarify this question.

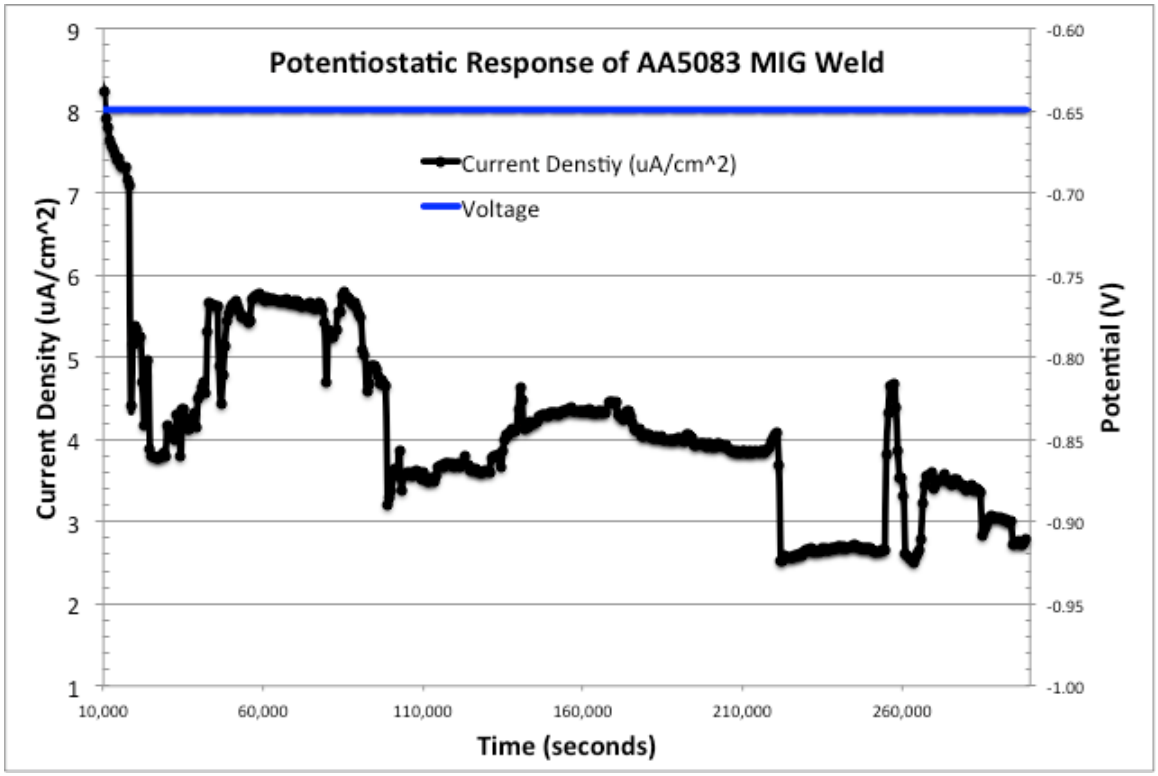

Figure 30. Potentiostatic test for combined samples of the control weld and laser peened weld 1-18-1.

D. DISCUSSION OF HYPOTHESES

Two research questions and their respective hypotheses guided the work in this thesis. The results of this thesis work have provided partial answers to these questions.

Does LP prevent SCC at fusion welds in AA5083?

Our hypothesis was that LP would help prevent SCC in fusion welds on AA5083. The answer to this question is ambiguous. We did not observe clear SCC behavior except in the control, highly sensitized material. We did observe a systematic reduction in strain-to-failure for increased laser peening; however, this observation stems more from the effect of cold work on weld metal than on its interaction with SCC. In fact, it is likely that if these measurements were repeated in air, the over all trend linking LP and ductility would be the same.

If overall ductility at welds is a key requirement for the alloy then care should be shown in determining how much laser peening should be used. For answering the question of SCC mitigation at welds, it seems that slow strain rate testing (SSRT) may not be the best test. Although SSRT is popular in the stress-corrosion literature, it is likely not the best measure of the effectiveness of LP on preventing SCC. As discussed below, future measurements should include more stress-controlled mechanical tests such as compact tension and corrosion fatigue testing.

How does LP alter the microstructure of the AA5083 material?

Our hypothesis was that LP would generate a large amount of plastic deformation in the microstructure. This plastic deformation will be manifested by a clear increase in hardness at the surface of the material and by a measurable increase in orientation spread within the aluminum grains themselves. This hypothesis was primarily correct as we did observe a marked increase in hardness, particularly in the weld-HAZ region of the specimens. The measurements to determine the orientation spread and residual stress levels are underway and will be addressed in future work.

D. FUTURE WORK

This master's thesis work is the beginning of an important compilation of science relevant to both the Navy and commercial marine fleet. One of the first things that need to be completed is to measure the residual stresses in both control welds and then laser peened welds. By measuring the residual stresses, more accurate fracture analyses can be by better specifying the nature and magnitude of the stress acting on the crack.

Further work needs to be pursued using stress-controlled mechanical testing. This testing includes stress-hold testing and potentiostatically driven cracking. The primary stress-driven test should be a self-loaded compact tension (CT) test, which will add additional tensile stress to the weld and more closely simulate a ship structure environment. Even more importantly, the CT test can be used to measure the K_{ISCC} value that is the true basis for predicting fracture behavior in a corrosive environment. Although not successful in this thesis, driving SCC with a potentiostat should be further pursued. This test is valuable because it always detailed electrochemical characterization

of the process that drives SCC in the welded material. Finally, a corrosion-fatigue testing on the laser peened material will complement the monotonically-loaded tests and will simulate the flexural natural of ship movement in a corrosive environment.

It also needs to be investigated if a laser peened sample will become sensitized again if exposed to elevated temperatures after extended amounts of time. It is important to know the response of a laser peened sample to a potentially sensitizing environment in order to determine the longevity of this surface treatment in a ship board environment. Further work also needs to investigate the effectiveness of laser peening in marine aluminum with existing cracks. A lot of the current problems related to this situation are on ships with existing cracks and a way to prevent the cracks from propagating further is greatly needed.

IV. CONCLUSIONS

This master's thesis has investigated the use of laser peening for suppression of stress corrosion cracking (SCC) in metal-inert-gas (MIG) welds in AA5083 (Al-Mg alloy) in a corrosive environment. Laser peening (LP) was applied to a series of MIG welds with systematic increases in laser power density, pulse duration, and number of passes. The effect of laser peening was investigated by both potentiostatic testing and slow strain rate testing (SSRT). Attempts to drive SCC using an applied potential in combination with the residual tensile stresses in the heat affected zone of the weld were unsuccessful. It is possible that MIG-welded 5083 is not sufficiently sensitized to cause SCC.

The SSRT results showed a systematic reduction in strain at failure with increasing LP intensity. The fracture surfaces all showed a pronounced pre-crack shelf, which reduced in size with increasing laser peening intensity. However, the fracture surfaces of the laser peened and control weld samples all showed primarily ductile failure with the exception of a control AA5083 plate sample that was sensitized in solution. The exact mechanism of the sub-critical crack growth remains to be determined. Statistical analysis of these results clearly demonstrated that the laser peening process variables all had significant, primary effects upon the strain to failure.

Laser peening increases the hardness of the material, particularly in the weld and heat affected zone areas. Statistical analysis of the hardness data demonstrated that only laser power density was a significant factor and that hardness increases with increasing laser power density. The increase in hardness is small in the base metal of a laser peened sample as compared with the control, rolled material. The increase in hardness is significantly greater in the weld-HAZ area. The fracture and hardness results indicate a complex interaction between the applied stress level, and K_c of the material, but seem to indicate an increase of LP will decrease the critical flaw length at the weld under monotonic loading to failure. These interactions may affect the local fracture toughness of the weld-HAZ material.

THIS PAGE INTENTIONALLY LEFT BLANK

LIST OF REFERENCES

[1] H. Bushfield and M. Cruder. *Sensitized Marine Aluminum Plate & ASTM Standard Specification B928-an Update*. in *SNAME Section Meeting*. 2006.

[2] M. G. P. Ammon, *NPS Student-Professor Team Assists Commander U.S. THIRD Fleet with 'Splitting' Dilemma*, in *NPS News*2011, NPS: Monterey, CA.

[3] C. P. Cavas, *Cracks Continue to Plague U.S. Cruisers*, in *Defense News*2010. p. 4.

[4] K. N. Tran, M. R. Hill, et al., *Welding Journal*, 85 (2006) 28.

[5] M. G. Fontana, *Stress Corrosion*, in *Corrosion Engineering*1987, Mc Graw Hill Book Co.: Singapore. p. 109.

[6] S. Kou, *Residual Stresses, Distortion, and Fatigue*, in *Welding Metallurgy*2003, John Wiley and Sons, Inc.: Hoboken, NJ. p. 122.

[7] M. James, D. Hughes, et al., *International Journal of Fatigue*, 31 (2009) 28.

[8] R. Jones and R. Ricker, *Stress Corrosion Cracking*, in *Stress Corrosion Cracking, Materials Performance and Evaluation*1992, ASM International: Materials Park, OH. p. 1.

[9] F. Zucchi, G. Trabanelli, et al., *Materials And Corrosion-Werkstoffe Und Korrosion*, 52 (2001) 853.

[10] I. N. A. Oguocha, O. J. Adigun, et al., *Journal Of Materials Science*, 43 (2008) 4208.

[11] A. International, *Standard Test Method for Determining the Susceptibility to Intergranualr Corrosion of 5XXX Series Aluminum Alloys by Mass Loss after Exposure to Nitric Acid*, 2004, ASTM International. p. 1.

[12] R. Jones and R. Ricker, *Stress Corrosion Cracking of Aluminum Alloys*, in *Stress Corrosion Cracking, Materials Performance and Evaluation*1992, ASM International: Materials Park, OH. p. 233.

[13] W. D. J. Callister, *Failure*, in *Materials Science and Engineering: an Introduction*2007, John Wiley and Sons, Inc.: York, PA. p. 236.

[14] M. Liao, W.R. Chen, et al., *International Journal of Fatigue*, 30 (2008) 717.

[15] O. Hatamleh, *International Journal of Fatigue*, 31 (2009) 974.

[16] J. Farmer, S. Lu, et al. *Modeling and Mitigation of Stress Corrosion Cracking in Closure Welds of High-Level Waste Containers for Yucca Mountain*. in *2000 ASME Pressure Vessel and Piping Conference*. 2000. Seattle, Washington.

[17] O. Hatamleh, P. M. Singh, et al., *Journal Of Materials Engineering And Performance*, 18 (2009) 406.

[18] P. Peyre, C. Carboni, et al., *Journal Of Materials Science*, 42 (2007) 6866.

[19] A. International, *Standard Practice for Slow Strain Rate Testing to Evaluate the Susceptibility of Metallic Materials to Environmentally Assisted Cracking*, 2006, ASTM INternational.

[20] W. Wen and J.G. Morris, *Materials Science And Engineering A-Structural Materials Properties Microstructure And Processing*, A354 (2003) 279.

[21] R. G. Petersen, *Response Surfaces*, in *Design and Analysis of Experiments*1985, Marcel Dekker: New York, NY. p. 252.

[22] J. L. Searles, P. I. Gouma, et al., *Aluminum Alloys 2002: Their Physical And Mechanical Properties Pts 1-3*, 396-4 (2002) 1437.

[23] R. W. Hertzberg, *Elements of Fracture Mechanics*, in *Deformation and Fracture Mechanics of Engineering Materials*1996, John Wiley & Sons: Hoboken, NJ. p. 315.

[24] M. A. Meyers and K. K. Chawla, *Hardness*, in *Mechanical Behavior of Materials*2009, Cambridge University Press: Cambridge, UK. p. 214.

INITIAL DISTRIBUTION LIST

1. Defense Technical Information Center
   Ft. Belvoir, Virginia

2. Dudley Knox Library
   Naval Postgraduate School
   Monterey, California

3. MAE Department Chairman,
   Dr. Knox Millsaps
   Naval Postgraduate School
   Monterey, California

4. Engineering and Technology Curricular Office, Code 34
   Naval Postgraduate School
   Monterey, California

5. Professor Luke N. Brewer
   Naval Postgraduate School
   Monterey, California

6. Dr. Joseph C. Farmer
   Directorate Senior Scientist
   National Ignition Facility & Photon Sciences
   Lawrence Livermore National Laboratory (LLNL)
   Livermore, California

7. LLNL Visiting Professor
   Mechanical and Aerospace Engineering Department
   Naval Postgraduate School
   Monterey, California